AD NUMBER

AD487477

LIMITATION CHANGES

TO:

Approved for public release; distribution is unlimited.

FROM:

**Distribution authorized to U.S. Gov't. agencies and their contractors;
Administrative/Operational Use; AUG 1966. Other requests shall be referred to Arnold Engineering Development Center, Arnold AFB, TN.**

AUTHORITY

AEDC ltr 23 Jan 1975

AEDC-TR-66-112

DESCRIPTION OF A MODEL LAUNCHER AND TECHNIQUES USED FOR OBTAINING MODEL FREE-FLIGHT MEASUREMENTS IN THE VKF CONTINUOUS FLOW WIND TUNNELS AT MACH NUMBERS FROM 1.5 THROUGH 10

L. K. Ward, A. E. Hodapp, Jr., and R. H. Choate
ARO, Inc.

August 1966

VON KÁRMÁN GAS DYNAMICS FACILITY
ARNOLD ENGINEERING DEVELOPMENT CENTER
AIR FORCE SYSTEMS COMMAND
ARNOLD AIR FORCE STATION, TENNESSEE

NOTICES

When U. S. Government drawings specifications, or other data are used for any purpose other than a definitely related Government procurement operation, the Government thereby incurs no responsibility nor any obligation whatsoever, and the fact that the Government may have formulated, furnished, or in any way supplied the said drawings, specifications, or other data, is not to be regarded by implication or otherwise, or in any manner licensing the holder or any other person or corporation, or conveying any rights or permission to manufacture, use, or sell any patented invention that may in any way be related thereto.

Qualified users may obtain copies of this report from the Defense Documentation Center.

References to named commercial products in this report are not to be considered in any sense as an endorsement of the product by the United States Air Force or the Government.

DESCRIPTION OF A MODEL LAUNCHER AND TECHNIQUES USED FOR OBTAINING MODEL FREE-FLIGHT MEASUREMENTS IN THE VKF CONTINUOUS FLOW WIND TUNNELS AT MACH NUMBERS FROM 1.5 THROUGH 10

L. K. Ward, A. E. Hodapp, Jr., and R. H. Choate
ARO, Inc.

AF AEDC
Arnold AFS Tenn

FOREWORD

The work reported herein was completed at the request of Headquarters, Arnold Engineering Development Center (AEDC), Air Force Systems Command (AFSC), under Program Element 65402234.

The results of research presented were obtained by ARO, Inc. (a subsidiary of Sverdrup & Parcel and Associates, Inc.), contract operator of AEDC, AFSC, Arnold Air Force Station, Tennessee, under Contract AF40(600)-1200. The work was done under ARO Project No. VT3444, and the manuscript was submitted for publication on May 11, 1966.

This technical report has been reviewed and is approved.

Rodney W. Brown
Captain, USAF
Research Division
Directorate of Plans and Technology

Donald D. Carlson
Colonel, USAF
Director of Plans and Technology

ABSTRACT

A model launcher has been developed for use in the continuous flow wind tunnels, Tunnels A, B, and C (Mach numbers from 1.5 through 10) of VKF. Support-free model drag, damping, and pitching-moment rate data may be obtained throughout the Mach number range. Model base pressure data, using onboard telemetry, may be obtained at Mach numbers up through 6. Repeated model launchings may be made without interrupting the tunnel flow. A description of the model launcher and testing procedures are presented with representative drag, damping, pitching-moment rate, and base pressure data obtained on 10-deg, half-angle cone models in free flight.

CONTENTS

ILLUSTRATIONS

NOMENCLATURE

A	Reference area (model base area), ft^2
$^{a}X_F$	Acceleration of the model center of gravity, relative to the media fixed axes system, in the X_F direction, ft/sec^2
$^{a}X_T$	Acceleration of the model center of gravity, relative to the tunnel fixed axes system, in the X_T direction, ft/sec^2
C_A	Total axial-force coefficient, $2F_A/\rho_\infty V^2A$
C_D	Total drag coefficient, $2D/\rho_\infty V^2A$
C_{D_B}	Base drag coefficient based on model base area
C_{D_p}	Inviscid pressure drag coefficient based on model base area
ΔC_{D_v}	Viscous drag coefficient, $C_D - (C_{D_p} + C_{D_B})$

C_m	Pitching-moment coefficient, $2M_Y/\rho_\infty V^2Ad$
C_{m_o}	Pitching-moment coefficient at $\alpha = 0$
C_{m_q}	$\partial C_m/\partial (qd/2V)$, 1/radian
C_{m_α}	$(\partial C_m/\partial \alpha)$, 1/radian
$C_{m_{\dot\alpha}}$	$\partial C_m/\partial(\dot\alpha d/2V)$, 1/radian
C_N	Normal-force coefficient, $2F_N/\rho_\infty V^2A$
C_{N_o}	Normal-force coefficient at $\alpha = 0$
C_{N_q}	$\partial C_N/\partial(qd/2V)$, 1/radian
C_{N_α}	$\partial C_N/\partial \alpha$, 1/radian
$C_{N_{\dot\alpha}}$	$\partial C_N/\partial(\dot\alpha d/2V)$, 1/radian
C_{Y_R}	Cycles to damp to a given amplitude ratio R
C_∞	Form of Chapman-Rubesin viscosity coefficient, $(\mu_w/\mu_\infty)\ (T_\infty/T_w)$
D	Drag, lb (see Fig. I-2)
d	Model base diameter, ft
d_s	Sting diameter, ft
$\bar{F}$	Vector resultant of external forces acting on the model $(F_X\bar{i} + F_Y\bar{j} + F_Z\bar{k})$, lb
F_X	Aerodynamic axial force $(-F_A)$, lb (See Fig. I-2)
F_Z	Aerodynamic normal force $(-F_N)$, lb (See Fig. I-2)
f_o	Telemeter center frequency, cps
g	Acceleration of gravity, ft/sec^2
$\bar{H}$	Angular momentum vector, ft-lb-sec
I	Mass moment of inertia, slug-ft^2
I_X, I_Y, I_Z	Mass moments of inertia about the X, Y, and Z axes, respectively, slug-ft^2
$\bar{i}$, $\bar{j}$, $\bar{k}$	Unit vectors in the X, Y, and Z directions, respectively
L	Inductance, h
ℓ	Model length, ft
$\bar{M}$	Vector resultant of external moments acting on the model $(M_X\bar{i} + M_Y\bar{j} + M_Z\bar{k})$, ft-lb
$\bar{M}$	Linear momentum, lb-sec

M_Y	Aerodynamic pitching moment, ft-lb (See Fig. I-2)
M_∞	Free-stream Mach number
m	Model mass, slug
N	Number of cycles of oscillation
p,q,r	Rolling, pitching, and yawing velocities, respectively, radians/sec (See Eq. (I-2))
Δp	Differential pressure, psi
p_b	Model base pressure, psia
p_r	Reference pressure, psia
p_∞	Free-stream pressure, psia
q_∞	Free-stream dynamic pressure, psia
R	Amplitude ratio, α_n/α_o
Re_ℓ	Free-stream Reynolds number, based on model length
r_b	Model base radius, in.
r_n	Model nose radius, in.
T	Temperature, °R
T_o	Stilling chamber total temperature, °R
t	Time, sec
Δt	Time interval, sec
u, v, w	Model velocities in the X, Y, and Z directions, respectively, ft/sec
V	Velocity of the model center of gravity with respect to the media, ft/sec
V_{X_F}	Velocity of the model center of gravity, relative to the media fixed axes system, in the X_F direction, ft/sec
V_{X_T}	Velocity of the model center of gravity, relative to the tunnel fixed axes system, in the X_T direction, ft/sec
V_∞	Free-stream velocity, ft/sec
$\bar{v}_\infty$	Viscous parameter, $M_\infty[C_\infty/Re_\ell]^{1/2}$
W	Model weight, lb
X, Y, Z	Body axes system

ΔX	Distance interval, ft
X_F	Distance from the media fixed axes system to the model center of gravity, ft (See Fig. I-1)
X_F, Y_F, Z_F	Media fixed axes system, parallel to the tunnel fixed axes system
X_m, Y_m, Z_m	Model fixed axes system, parallel to the tunnel fixed axes system
X_T	Distance from the tunnel fixed axes system to the model center of gravity, ft (See Fig. I-1)
X_T, Y_T, Z_T	Tunnel fixed axes system (inertial reference)
α	Angle of attack, deg or radians
α_m	Mean angle of attack, deg or radians
β	Angle of side slip, deg or radians
γ	Arbitrary phase angle, radians
Δ	Logarithmic decrement
δ	Effective angle of attack, radians or deg (See Eq. (I-19))
θ	Angle of pitch, deg or radians (See Fig. I-2)
θ_c	Cone half-angle, deg
μ	Air viscosity, lb-sec/ft^2
ρ_∞	Free-stream density, slug/ft^3
σ	Radius of gyration, ft
ψ, θ, ϕ	Euler angles, radians
Ω	Angular frequency, radians/ft
ω	Angular frequency, radians/sec
$\bar{\omega}$	Vector angular velocity of the body axes system with respect to the model fixed axes system and inertial space, $(p\bar{i} + q\bar{j} + r\bar{k})$
$\omega d/2V_\infty$	Reduced frequency parameter, radians
$(\dot{}), \quad (\ddot{})$	First and second derivatives with respect to time, t
$(')$, $('')$	First and second derivatives with respect to distance, X_F

SUBSCRIPTS

E	Effective values
n	Number of cycles of oscillation during the data interval
o	Conditions at the beginning of the data interval (initial conditions)
w	Model wall conditions
∞	Free-stream conditions

SECTION I
INTRODUCTION

A developmental program has been conducted at the von Kármán Gas Dynamics Facility (VKF), AEDC, to provide free-flight model testing capabilities in the VKF continuous flow tunnels. The objectives of this program were to provide an additional means of testing models in the VKF wind tunnels and to obtain damping, drag, pitching-moment rate, base pressure, and base heating data from models in free flight.

Data have been obtained from models in free flight at many wind tunnel facilities. Allen of NACA proposed to gun-launch models at high speeds upstream through the test section of a supersonic wind tunnel and obtain hypersonic flow about the test model. This proposal resulted in the development of the Ames supersonic free-flight wind tunnel as reported by Seiff in Ref. 1. More recently, free-flight data have been obtained in shock tunnels (Refs. 2 and 3) and in "hot-shot"-type tunnels (Ref. 4) using models initially supported by threads which were blown free during the tunnel starting process. Kinslow and Potter (Ref. 5) employed a technique which allowed the model to fall into the tunnel flow and obtained drag data from the model's time history.

Dayman (Ref. 6) showed that models could be successfully suspended by wires in conventional tunnels and released after the tunnel flow was established. Dayman went further (Ref. 7) to launch models by means of a pneumatically operated launcher which propels the test model upstream into the test section until the model drag overcomes its upstream momentum and the model moves downstream. If the model drag and upstream velocity are properly balanced, the time for model viewing is essentially double that for a wire released model. This feature has practical importance when gathering data by photographic means in order to study model motion-time histories.

A pneumatically operated model launcher was developed under the VKF program for use in the 40-in. supersonic tunnel (Gas Dynamic Wind Tunnel, Supersonic (A)) and the 50-in. hypersonic tunnels (Gas Dynamic Wind Tunnels, Hypersonic (B) and (C)). The combined operating Mach number range of these continuous flow tunnels is from 1.5 through 10. The launcher provides a means of obtaining model drag and stability data in Tunnels A, B, and C and telemetered base pressure data in Tunnel A.

During the course of the development, a model drop technique was developed for use in Tunnels B and C to obtain model base pressure and base heating measurements by means of telemetry at Mach 6, 8, and 10.

This technique, which allows repeated testing of one model without interrupting the tunnel flow, is described in detail in Ref. 8.

SECTION II
APPARATUS

2.1 WIND TUNNELS

Tunnels A, B, and C are continuous, closed-circuit, variable density wind tunnels. Tunnel A (Fig. 1a) has a flexible-plate-type nozzle which is automatically driven to produce Mach numbers from 1.5 to 6. The tunnel has a 40- by 40-in. test section and operates at maximum stagnation pressures ranging from about 29 to 200 psia at M_∞ = 1.5 to 6, respectively, and at stagnation temperatures up to 300°F (M_∞ = 6). Minimum operating pressures are about one-tenth of the maximum.

Tunnels B (Fig. 1b) and C (Fig. 1c) have contoured axisymmetric nozzles and 50-in. test sections. Tunnel B operates at Mach 8 at stagnation pressures ranging from 100 to 800 psia and at stagnation temperatures up to 900°F and at Mach 6 at stagnation pressures ranging from 20 to 300 psia at stagnation temperatures of 390°F. Tunnel C operates at Mach 10 with stagnation pressures ranging from 200 to 2000 psia and at stagnation temperatures up to 1450°F.

2.2 LAUNCHER SYSTEMS

The pneumatically operated model launcher and its associated support systems were designed primarily to obtain repeatability in model launch velocity and to have the capability of consecutive model launchings with continuous tunnel operation. The launcher is mounted on a support which can be injected into the tunnel flow. This injection/retraction sequence begins and ends in an enclosure which can be isolated from the tunnel flow to either reload models or service the launcher. Two separate launcher supports were developed, one for use in Tunnel A and the other for use in Tunnels B and C.

2.2.1 Model Launcher

The pneumatically operated launcher, shown in Fig. 2, is composed of a water-cooled stainless steel case, an aluminum piston, a stainless steel piston guide, and a pressure reservoir. The pressure reservoir, attached to the launcher case, has a volume which is several orders of

magnitude greater than the volume of the piston; therefore, changes in volume caused by movement of the piston are negligible.

In Fig. 3, the launcher charging and firing processes are diagrammed. The piston is placed firmly against the O-ring, and the enclosed volume behind the piston is vented to vacuum conditions (Fig. 3a), which results in a force on the piston directed to the right, thus fixing its position. The pressure within the reservoir and launcher body is then raised from atmospheric to the desired launch pressure (Fig. 3b). To fire the launcher, the reservoir tank is vented into the O-ring enclosed volume (Fig. 3c). This equalizes the pressure everywhere within the launcher, causing a constant force on the piston which results in a launch (Fig. 3d).

2.2.2 Model Launcher Adapter

Model adapters, bolted to the forward portion of the piston (Fig. 2), are easily interchangeable. The adapters used in this investigation are shown in Fig. 4.

The pressure model adapter (Fig. 4a) is channeled to connect the model's pressure port to the reference pressure tube (Fig. 2). Pressure models are supported by the cylindrical portion of this adapter and by dowels which are anchored in the launcher body and extend through the adapter into the model. The cylindrical portion of the adapter also provides a surface for sealing the model reference pressure cavity.

Channels in the drag and moment model adapters (Figs. 4b and c) provide a means of reducing the model internal pressure which aids in holding the model on the adapter. The adapters are conical frustrums whose outer surfaces mate with the inner model wall.

In order to obtain pitching motion after launch, the moment model adapter was built with its centerline inclined at a 10-deg angle. The drag model adapter was built for zero angle-of-attack releases; therefore, its axis of symmetry and that of the piston were coincident.

2.2.3 Launcher Support Systems

The Tunnel A launcher support system, shown in Fig. 5, is an injection/retraction mechanism which is attached to a window opening on the outside wall of the tunnel. It consists of an actuator, a sliding valve, and a model housing. As shown in Fig. 5, the actuator is a piston-cylinder device with the interior of the actuator shaft serving as the launcher pressure reservoir. With the launcher retracted and the

sliding valve closed, the model housing is isolated from the tunnel flow. Pressure within this housing can be set at either atmospheric or tunnel static pressure. The access hatch, located on the housing, can be removed to reload models (Fig. 6). Figure 7 shows the system installed on Tunnel A. In the bottom right-hand corner of this figure is the control panel from which the system is operated.

Operation of the actuator is demonstrated in Fig. 8 as viewed from within Tunnel A. In Fig. 8a, the sliding valve is open with the launcher still contained in the model housing. Figure 8b shows the actuator fully extended with the launcher in the flow ready to fire.

Shown in Fig. 9 is the water-cooled launcher support system used in Tunnels B and C. The launcher support is attached directly to the Tunnel B and C injection/retraction systems which are used to inject the launcher from, and retract it into, a tank located directly below the tunnel test section (Figs. 1b and c). The tank can be vented to atmospheric pressure and opened to reload models without interrupting the tunnel flow. Figure 10 shows the launcher system in Tunnel C in its retracted and injected positions.

2.2.4 Model Catchers

Model catchers are used with both launcher systems. The catchers are simple boxes framed with stainless steel and covered with wire cloth. The cloth grid was small enough to prevent models from escaping the catcher, yet large enough to prevent complete blockage of the flow.

The primary use of the Tunnel A model catcher (Fig. 11) is to recover telemetry packages. A nylon net, placed inside the model catcher, is used to cushion the impact of models containing telemetry packages. These recovered packages, in most cases, could be reused after minor repair.

The Tunnel B and C model catcher (Figs. 10a and 12) is used primarily to protect downstream tunnel components. No gun-launched free-flight telemetry shots are made in these tunnels because a free-flight drop technique, as described in Ref. 8, is available. Figure 13 gives the relationships between the positions of the launcher, the model catchers, and the upstream limits of the viewing area for the systems.

2.3 MODELS

The models used in this investigation were sharp, 10-deg, half-angle cones designed and built at VKF. Free-flight testing requires

models specifically tailored to perform certain desired motions in order to maximize data quality. For this reason three separate model designs were used to obtain model drag, moment, and base pressure data. As a result of the small structural loads occurring from low launch and flight accelerations (10 to 100 g), models could be constructed simply and with great latitude in weight and center-of-gravity variations.

Materials used to form the aerodynamic contour of the models were different for the supersonic and hypersonic tests. Magnesium and Grade A Lava® were used for the hypersonic tests, and Lexan® (a polycarbonate plastic) was used for the supersonic tests. The Lava models were used primarily to check the placement of the model catcher. They disintegrated upon impact and reduced the possibility of damage to downstream tunnel components.

2.3.1 Drag Models

Drag model design is governed by the equation of horizontal translatory motion

$$a_{X_F} \simeq \frac{C_D \, q_\infty \, A}{m}$$

where it is assumed that $V \simeq V_\infty$. From this equation it is evident that for a fixed model size the model mass is the only model parameter that can be varied. The accuracy of drag measurements is maximized at a given tunnel condition by obtaining the largest model acceleration (a_{X_F}) compatible with high speed photographic capabilities.

The drag model designs used in the supersonic and hypersonic investigations are given in Fig. 14. Both model types were formed of a thin-walled, open afterbody and a solid nose section. The desired mass and stability margin were obtained by varying the nose section length. Using this method, stability margins ranging from 0.02 to 0.22 body lengths could be obtained with model weights ranging from 0.062 to 0.12 lb.

2.3.2 Moment Models

When designing models to measure the damping-moment and pitching-moment slope, it is desirable to minimize the logarithmic decrement and to maximize both the number of cycles of motion and the time of flight for a given flight distance. Using simplified forms of the equations of motion (assume $\theta = \alpha$ and that $V \simeq V_\infty$) yields the following relations:

$$\Delta = \frac{\pi\sqrt{q_\infty}}{2V_\infty} \left(C_{m_q} + C_{m_{\dot{\alpha}}}\right) \left\{ \frac{1}{C_{m_\alpha}} \left(\frac{A d^3}{I}\right) \right\}^{1/2}$$

$$N = \frac{1}{\pi}\left\{-\frac{C_{m_\alpha}}{C_D}\frac{X_{Td}}{2}\left(\frac{m}{I}\right)\right\}^{1/2}$$

$$t = \left\{\frac{2X_T m}{C_D q_\infty A}\right\}^{1/2}$$

From these relations it is seen that for a given size model, these objectives are achieved by maximizing the mass and minimizing the moment of inertia. Model size should also be considered; however, it is usually governed by other requirements.

Moment model design for these investigations is given in Fig. 15. The m/I parameter of these models was maximized by using a light material to form a thin-walled aerodynamic contour and by using a heavy material concentrated at the center of gravity. The model core was threaded so that the model center of gravity could be easily positioned at the desired location.

2.3.3 Base Pressure Models

The base pressure models used in this investigation (Fig. 16) were constructed similar to the supersonic drag models with the addition of a base plate on which the telemetry package is mounted. The length of the metal model nose was limited by the physical dimensions of the telemetry package. This restriction on nose length, combined with the large weight of the telemetry package acting behind the desired model center of gravity, limited the maximum static margin to about 0.08 body lengths.

2.4 TELEMETRY INSTRUMENTATION

2.4.1 Receiving and Recording Equipment

A high frequency, FM receiver, tunable from 55 to 260 mc and having a nominal discriminator bandwidth of ±600 kc, was used throughout these tests. The discriminator was modified to provide a d-c output voltage which was proportional to frequency deviation produced by a differential pressure application and was recorded on an oscillograph. Another receiver output, which was a function of the strength of the received RF signal, was also recorded. This gave a continuous record of telemeter signal strength throughout a data run, so that any erroneous data resulting from low signal strength might be recognized. Stub antennas, approximately one-quarter wavelength long and located on the

tunnel windows, provided satisfactory signal pickup. Two antennas were used, one near the model injection system and one near the free-flight zone. These antennas were paralleled directly into the receiver and no pre-amplification was required.

2.4.2 Telemeters

2.4.2.1 Circuitry

The telemeters used in these tests were Clapp-type oscillators (Ref. 9) operating in the 160- to 180-mc frequency range. Variable capacitance-type pressure transducers provided direct frequency modulation as a function of differential pressure across the transducer (Fig. 17). This Clapp configuration was chosen because the Colpitts-type telemeters previously used (Refs. 8 and 10) required shielding to prevent extraneous frequency shifts caused by proximity effects, whereas the Clapp type did not. Current drain was nominally 1 ma from the 5.4-v source.

Telemeter sensitivities to differential pressures applied to the transducers were adjusted to nominally 60 kc/0.01 psid by the addition of a 10-pf padder capacitor across the transducer (Fig. 17). This sensitivity setting provided a differential pressure range coverage of nominally ±0.05 psid. The maximum sensitivity available from this telemeter (no padder capacitor) is nominally 60 kc/0.003 psid.

2.4.2.2 Transducers

A sketch of the variable-capacitance differential pressure transducer is shown in Fig. 18. Quiescent capacitance of this transducer is nominally 10 pf. A capacitance change of nominally 0.6 pf results from the application of 0.1 psid. The transducer diaphragm is prestressed over the support diameter of the case and affixed by a series of overlapping spot welds to form a pressure-tight seal. Response time of this transducer to a pressure step of 0.1 psia applied to the pressure port is less than 2 msec. A pressure-lag system incorporated in the reference pressure side of the transducer maintains reference pressure at an essentially constant value during the free-flight period. The application of a 0.1-psia step to the reference pressure port results in a reference pressure change at the diaphragm of 1 percent or less in 200 msec. During the free-flight tests, the pressure measurement and reference ports of the transducer were both connected to the same model base pressure orifice.

2.4.2.3 Construction Techniques

Telemeter packages, cast in lightweight (specific gravity ≈ 0.85) epoxy resin for shock and thermal isolation, were secured to the model base plate. Additional thermal isolation was provided by an air space between telemeter package and model wall. Pressure routing systems were required in the telemeter package to connect both transducer ports to a common base pressure orifice, as described previously. However, independent access to the transducer ports was required for static calibrations. The method used to allow static calibrations is outlined in Fig. 19, which shows the pressure routing systems contained within the telemeter. Calibrations were performed before the base plate was permanently secured. The plastic and steel tubing inserted into the pressure passage formed a satisfactory pressure seal for isolation between transducer ports during calibration. It was assumed that relatively large diameter pressure routing channels did not contribute to the pressure lag of the system. This was based on a measured lag (transducer only) of about 10 msec through 4 in. of 0.032-ID tubing with a 0.1-psia pressure step applied.

Figure 20 shows telemeter packages during various stages of construction. The molded epoxy resin cylinder containing the pressure routing systems was modified to accept the transducer. After sealing the transducer in place, the circuitry was constructed on top of the transducer, after which the final molding was performed.

SECTION III
PROCEDURE

3.1 PRELIMINARY TESTS

3.1.1 Launcher Calibration

The launcher was calibrated prior to the tunnel tests to determine the relationship between reservoir pressure and launch velocity for given masses. Only the lower third of the launcher's capability was calibrated, since this range more than adequately covered all of the necessary test conditions.

The calibration procedure consisted of launching spheres of a known mass through two parallel light beams located a known distance apart. A digital counter, used in conjunction with two photocells, recorded the elapsed time between interruptions of the light beams. The results of the

calibrations are shown in Fig. 21. Over the range of variables calibrated, the launcher proved to be repeatable to within about 1 ft/sec.

3.1.2 Model Parameter Measurements

Prior to the tunnel tests, all model parameters necessary for data reduction and for determining launch conditions were measured. The longitudinal center-of-gravity position and lateral mass moment of inertia were determined only for the moment models.

All model dimensions were determined to within 0.001 in. The model mass was determined to 0.0001 gm using a precision analytical balance. Measurements of model center-of-gravity position and moment of inertia were made using a beam-balance device and a torsional pendulum device, respectively. By using these systems, the center of gravity of a precisely constructed model can be determined to within ±0.002 in., and the moment of inertia can be determined to within ±0.20 percent.

3.1.3 Telemeter Calibrations

The entire pressure telemeter package was placed in a bell jar and maintained at some arbitrary reference pressure near 1 psia during static calibrations. Spot checks at reference pressures between 0.002 and 4 psia were made to verify that no calibration sensitivity changes arose from changes in ambient pressure level. Differential pressures applied to the telemeters were verified with a precision micromanometer having a nominal resolution of ±0.000067 psid.

The pressure telemeters used in these tests required calibration with both increasing and decreasing pressure differentials. A sweep pressure technique was devised to perform these calibrations. A sketch of this calibration system is shown in Fig. 22. The desired reference pressure was established in both bell jars, with no differential pressure between jars. The pressure in the bell jar common to the transducer reference port (lag system) was then increased until telemeter frequency deviation (and resulting galvanometer deflection) was approximately (minus) full scale. After the transducer's lag system had equalized, the bleed valve to the nonreference bell jar (common to the transducer's pressure port) was opened. As a result, the differential pressure applied to the telemeter would sweep from (minus) full scale, through zero, to (plus) full scale, resulting in a complete, continuous calibration plot. Two wafer gages (Ref. 11), whose calibrations were established using the micromanometer, allowed the differential pressure applied to the telemeter at any instant to be determined. A sample sweep calibration trace for one of these telemeters is shown in Fig. 23. Sweep and

point-by-point calibration techniques were found to yield identical results; however, calibration times were reduced by as much as 75 percent using the sweep method.

Pre-test telemeter calibration repeatabilities within 2 percent of reading were typical. Post-test calibration checks generally were not performed because the battery pack was usually broken off at a weak point in the package structure (see Fig. 20). However, the installation of new batteries showed calibrations generally to be within 5 percent of pre-test values.

3.2 TUNNEL TESTING

3.2.1 Drag and Moment Measurements

Model drag, damping, and pitching-moment rate measurements are obtained by analyzing the model motion-time histories. These histories are obtained by photographic means. Models which are launched at zero angle of attack may be photographed using a multiexposure technique which produces several model exposures on a single 8- by 10-in. photographic plate. The prime advantage of this technique is that one photograph may be used to obtain the model's trajectory. One disadvantage in using the technique is that nonparallel light produces parallax; however, the amount to be expected may be easily measured. Prior to each tunnel run, several photographic plates are exposed to a series of white grid lines on a black background which are located on the tunnel centerline. These pre-exposed plates are then used to photograph the model's flight (Fig. 24).

Models which are launched at an initial angle of attack to obtain damping data may be photographed using this technique; however, considerable overlapping of the model images occurs, and the resolution in measuring angle of attack is greatly decreased. An example of this is shown in Fig. 24b. All data on oscillating models were obtained by using a high speed (4000-frames/sec) 16-mm motion-picture camera.

3.2.1.1 Drag Data Reduction

The translational equation of motion developed in Appendix I for a model decelerating in free flight is given as

$$\dot{V} \simeq -\rho_{\infty} \frac{V^2 A}{2m} C_D$$

Forms of this equation from which the drag coefficient may be extracted using information obtained in the free-flight tests are given with respect

to the tunnel fixed coordinate system and media fixed coordinate system, respectively, as

$$C_{D_E} = \frac{2m}{\rho_\infty A V_{X_F}^2} a_{X_T}$$

and

$$C_{D_E} = \frac{-2m}{\rho_\infty A} \frac{\partial}{\partial X_F} \left[ln \left(1 + \frac{V_{X_T}}{V_\infty} \right) \right]$$

where

$$X_F = V_\infty t + X_T$$

and

$$V_{X_F} = V_\infty + V_{X_T}$$

Drag data were reduced using both of the above relations, and the agreement was excellent.

The X_T versus t curve (Fig. 25) obtained from the photographs was differentiated to obtain a_{X_T} and V_{X_T} as a function of time. These relationships were substituted into the preceding equations to obtain the drag coefficient as a function of time or distance. Effective angles of attack were obtained for these drag coefficients by the relation

$$\delta = \left\{ \frac{\alpha_n^2 - \alpha_0^2}{4 \, ln |\alpha_n / \alpha_0|} \right\}^{1/2}$$

3.2.1.2 Pitching-Moment Data Reduction

Neglecting the effects of gravity and assuming $C_{m_0} = C_{N_0} = 0$, the equation of planar free-flight angular motion is given in Appendix I as

$$\alpha'' + D_1 \alpha' + D_2 \alpha = 0$$

The dimensionless damping-in-pitch derivative coefficients and pitching-moment slope coefficient were obtained from each model flight using the amplitude-distance history (Fig. 26) and the following relations.

$$\alpha = \alpha_0 e^{\frac{-D_1}{2} X_F} \cos (\Omega X_F + \gamma)$$

where

$$\Omega = \sqrt{D_2}$$

$$D_1 = -2 \Omega \, ln \, R / 2\pi \, C_{Y_R}$$

$$C_{m_q} + C_{m_{\dot{\alpha}}} = 2 \left(\frac{\sigma}{d} \right)^2 \left[\frac{-2 D_1 m}{\rho_\infty A} - 2C_D + C_{N_\alpha} \right]$$

$$C_{m_\alpha} = \frac{-2md}{\rho_\infty A}\left(\frac{\sigma}{d}\right)^2 \Omega^2$$

Damping-moment coefficients were evaluated using C_{N_α} values obtained from conical flow theory.

To check results obtained by this method, data were also reduced using time as the independent variable by assuming that $V \simeq V_\infty$. This constant velocity assumption was valid for these tests since V_T was about 1 percent of V_∞.

The previous relationships may then be written as

$$\alpha = \alpha_0 e^{-\frac{C_1}{2}t} \cos(\omega t + \gamma)$$

where

$$\omega = \sqrt{C_2}$$

$$C_1 = -2\omega \ln R/2\pi C_{Y_R}$$

$$C_{m_q} + C_{m_{\dot\alpha}} = 2\left(\frac{\sigma}{d}\right)^2\left[\frac{-2C_1 m}{\rho_\infty V_\infty A} - C_D + C_{N_\alpha}\right]$$

$$C_{m_\alpha} = \frac{-2md}{\rho_\infty V_\infty^2 A}\left(\frac{\sigma}{d}\right)^2 \omega^2$$

The mean amplitude of oscillation for the data interval ($\Delta X_F = 2\pi C_{Y_R}/\Omega$ or $\Delta t = 2\pi C_{Y_R}/\omega$) over which these coefficients were obtained was evaluated by the following:

$$a_m = \left\{\frac{a_n^2 - a_0^2}{2 \ln \left| a_n/a_0 \right|}\right\}^{1/2}$$

3.2.2 Base Pressure Measurements

The procedure used for obtaining the model base pressure data was to install the model on the launcher and regulate the transducer reference pressure until the desired level was reached. Normally, this reference pressure was set at a value corresponding to the expected model base pressure, thus minimizing the Δp change. Once the reference pressure had stabilized, the $\Delta p = 0$ condition for the telemeter-transducer was established. The model was then injected into the tunnel, and after the receiver tuning was checked, the launch was initiated.

The output of the telemeter was recorded on an oscillograph, and the model reference pressure was recorded with tunnel transducer instrumentation. A high speed camera was used in conjunction with the tunnel

schlieren system to record the model attitude during the time of the base pressure data acquisition. The measured Δp, when added algebraically to the model reference pressure, yields the model base pressure.

During the tests in Tunnel A, the model was attached to the launcher in a manner which provided an O-ring seal from the reference pressure line to the base of the model. In addition, the model was held in place by two dowel pins as described in Section 2.2.2. During the release of the model at the end of the piston stroke, the O-ring was forced to slide free of the model adapter, thus inducing the possibility of the model separating at an angle of attack other than zero. Some of the runs showed the model to be oscillating at small angles of attack ($\alpha < 2$ deg). Base pressure data from the same runs indicated the model base pressure to be oscillating also.

Tests performed on the pressure telemeters used for data acquisition indicated that acceleration effects may be ignored in the data presented herein. Tests conducted both with the transducer at atmospheric pressure and at 0.1 torr showed that no significant difference in acceleration effects occurred as a function of absolute pressure. The results indicated that accelerations perpendicular to the diaphragm produce an output corresponding to a pressure reading of nominally 0.0002 psid/g, whereas accelerations parallel to the diaphragm contribute an output corresponding to about 0.00004 psid/g. Transducer diaphragms were oriented in the models parallel to the launch acceleration vector. For this orientation, acceleration effects correspond to a maximum readout error of about 0.00025 psid for the maximum axial deceleration during free flight or a maximum of about 0.0003 psid for a ±6-deg model oscillation at 12 cps.

Telemeter operating frequency and output sensitivity (kc/psid) are both functions of temperature. Operating frequency varies with temperature at a rate of about 25 kc/°F (0.0015 percent/°F of absolute frequency or about 4 percent/°F of data bandwidth), whereas sensitivity changes are about 0.2 percent/°F (Ref. 10). A series of models was exposed to the tunnel flow prior to launching for several minutes, and no telemeter center frequency drifts were observed. Errors from this source were considered negligible during the normal launch cycle.

SECTION IV
RESULTS AND DISCUSSION

The models used in the present tests to obtain free-flight drag, damping, pitching-moment rate, and base pressure data were all sharp,

10-deg, half-angle cones having a base diameter of 2 in. These data were obtained in both Tunnels A and C; however, no base pressure tests were attempted in Tunnel C using the model launcher, since these data may be obtained in the manner described in Ref. 8.

4.1 MODEL DRAG MEASUREMENTS

Drag data obtained during the tests in Tunnels A and C are shown in Fig. 27 as the effective drag coefficient (C_{D_E}) versus the mean square angle of attack (δ^2). These data show the expected trend of increasing drag with model angle of attack. The Mach 4 data show a more rapid rise with angle of attack than is expected; however, these data were obtained at a Reynolds number where model base drag is changing with angle of attack.

Zero angle-of-attack drag data are shown in Fig. 28 as a function of Mach number and are compared with data obtained from Ref. 12. As may be seen, the data agree well with the inviscid pressure drag plus base drag at $M_\infty = 4$; however at $M_\infty = 10$ the agreement is not good since a viscous drag is present. Figure 29 shows free-flight drag data obtained at $M_\infty = 10$ as a function of Reynolds number. The inviscid pressure drag is about 65 percent of the total drag, and the base drag is about 7 percent of the total. The remaining portion of the total drag is attributable to viscous effects.

Figure 30 shows the viscous drag coefficient (ΔC_{D_v}) as a function of the hypersonic viscous parameter ($\bar{v}_\infty$) (proposed by Whitfield and Griffith in Ref. 13). The present data and previous Tunnel C results (Ref. 14) and data from Ref. 15 are compared with predictions of viscous drag based on conical shock theory (Ref. 16) as outlined in Ref. 14. The agreement of the present data with theory and the referenced data is good.

4.2 MODEL MOMENT MEASUREMENTS

Model damping and pitching-moment rate data are shown in Fig. 31 for Mach 4 and 10 as the effective damping-in-pitch derivatives and the effective pitching-moment curve slope versus the mean angle of attack. The Mach 4 damping data (Fig. 31a) are compared with data obtained by Uselton in Ref. 17 with a sting-mounted model and show good agreement. Both sets of experimental data are in good agreement with Brong's flow field theory (Ref. 18) but are somewhat higher than Tobak's potential flow theory (Ref. 19). The Mach 4 pitching-moment data obtained during the tests increase with angle of attack. This increase is unexplained at

this time. The lower amplitude data agree well with conical flow theory and with Uselton's results.

The Mach 10 data (Fig. 31b) show excellent agreement with data from Ref. 20, obtained with a sting-mounted model, and with both flow field theory (damping data) and conical flow theory (pitching-moment data).

4.3 MODEL BASE PRESSURE MEASUREMENTS

Model base pressure data were obtained using telemetry from models in free flight in Tunnel A at Mach 4. Sketches from typical runs representing the variation of an increment of model base pressure (Δp) with time are shown in Fig. 32. Shown is a sketch of model base Δp having only a slight oscillation and one which shows a rather large Δp oscillation. The data were obtained at $Re_\ell \approx 2 \times 10^6$ and are compared in Fig. 33 with data from a sting-supported model tested in Tunnel A. All of the free-flight data obtained at this Reynolds number have Δp oscillation amplitudes which range between those shown in Fig. 32. The data points shown in Fig. 33 represent the maximum P_b/P_∞ obtained during the run and correspond to $\alpha = 0$, and the bar extending below the points represents the range of the pressure variation caused by angles other than zero.

The model oscillation amplitudes were less than 2 deg, and the frequency was twice that of the Δp oscillation. This is to be expected, since the base pressure variation with angle of attack (small angles) would peak at zero angle of attack and would be a minimum at the greatest angle of attack. The results in Fig. 33 show that the free-flight data obtained at a Reynolds number ($Re_\ell \approx 2 \times 10^6$) correspond to the case where the near wake is transitional. When transition is located in the near wake at $\alpha = 0$, it will move toward the base on the leeward side as the model is pitched. This will cause the model base pressure to decrease. Figure 34 shows the variation of P_b/P_∞ with angle of attack for a sting-supported, 10-deg, half-angle cone at $M_\infty = 4$. These data were obtained at a Reynolds number ($Re_\ell = 2.62 \times 10^6$) where transition is very near but downstream of the model base at $\alpha = 0$.

SECTION V
CONCLUDING REMARKS

A means of obtaining free-flight data in the VKF continuous flow tunnels has been developed. Model drag, damping, and pitching-moment rate data may be measured at Mach numbers ranging from 1.5 through 10. Model base pressure data may be measured at Mach

numbers ranging from 1.5 through 6. Repeated model launching may be made without interrupting tunnel operation. Data obtained during the system evaluation show good repeatability in the measurements and good agreement with theoretical predictions.

REFERENCES

1. Seiff, A. "A Free-Flight Wind Tunnel for Aerodynamic Testing at Hypersonic Speeds." NACA Report 1222, 1955.
2. Seigel, A. E. "Millisecond Measurements of Forces and Moments in Hypersonic Flow." NOLR 1238, NOL Aeroballistic Research Facilities Dedication and Decennial, May 1959.
3. Geiger, R. E. "Experimental Lift and Drag of a Series of Glide Configurations at Mach Numbers 12.6 and 17.5." Journal of Aerospace Sciences, Vol. 29, No. 4, April 1962, pp. 410-419.
4. Lukasiewicz, J. et al. "Development of Capacitance and Inductance Driven Hotshot Tunnels." AEDC-TN-60-222 (AD249421), January 1961.
5. Kinslow, M. and Potter, J. L. "The Drag of Spheres in Rarefied Hypervelocity Flow." AEDC-TDR-62-205 (AD290519), December 1962.
6. Dayman, B., Jr. "Simplified Free-Flight Testing in a Conventional Wind Tunnel." JPL Tech. Report 32-346, October 1962.
7. Dayman, B., Jr. "Free-Flight Hypersonic Viscous Effects on Slender Cones." AIAA Preprint 64-66, January 1964.
8. Ward, L. K. and Choate, R. H. "A Model Drop Technique for Free-Flight Measurements in Hypersonic Wind Tunnels Using Telemetry." AEDC-TR-66-77 (AD481967), May 1966.
9. Gartner, W. W. Transistors: Principles, Design, and Applications. van Nostrand Company, Inc., Princeton, New Jersey, 1960, p. 556.
10. Choate, R. H. and Young, R. P. "Radio Telemetry of Pressure and Heat-Transfer Data from Wind Tunnel Models in Free Flight." AEDC-TR-66-102 (AD481767), May 1966.
11. Smotherman, W. E. "A Miniature Wafer-Style Pressure Transducer." AEDC-TR-60-11 (AD243875), October 1960.

12. Jaffee, Peter and Prislin, Robert H. "Effect of Boundary-Layer Transition on Dynamic Stability." Journal of Spacecraft and Rockets, Vol. 3, No. 1, January 1966.

13. Whitfield, J. D. and Griffith, B. J. "Viscous Effects on Zero-Lift Drag of Slender Blunt Cones." AEDC-TDR-63-35 (AD298278), March 1963.

14. Whitfield, J. D. and Griffith, B. J. "Viscous Drag Effects on Blunt Slender Cones." AIAA Journal, Vol. 2, No. 10, October 1964.

15. Dayman, B., Jr. "Hypersonic Viscous Effects on Free-Flight Slender Cones." AIAA Journal, Vol. 3, No. 8. August 1965.

16. Probstein, R. F. "Interacting Hypersonic Laminar Boundary-Layer Flow over a Cone." TR AF 2798/1, Division of Engineering, Brown University, Armed Services Technical Information Agency, AD 66 227, March 1955.

17. Uselton, B. L. "Investigation of Sting Support Interference Effects on the Dynamic and Static Stability Characteristics of a 10-deg Cone at Mach Numbers 2.5, 3.0, and 4.0." AEDC-TDR-64-226 (AD450660), November 1964.

18. Brong, E. A. and Rie, H. "The Flow Field about Pointed and Blunt Bodies of Revolution in Unsteady Supersonic Flight." Transactions of the Second Technical Workshop on Dynamic Stability Testing, Vol. I (AD471665), Arnold Air Force Station, Tennessee, April 20-22, 1965.

19. Tobak, M. and Wehrend, W. R. "Stability Derivatives of Cones at Supersonic Speeds." NACA TN 3788. September 1956.

20. Hodapp, A. E., Jr., Uselton, B. L., and Burt, G. E. "Dynamic Stability Characteristics of a 10-deg Cone at Mach Number 10." AEDC-TDR-64-98 (AD440188), May 1964.

21. Murphy, C. H. "Free-Flight Motion of Symmetric Missiles." BRL Report 1216, July 1963.

22. Cassanto, J. M. "Effect of Cone Angle and Bluntness Ratio on Base Pressure." AIAA Journal, Vol. 3, December 1965, pp. 2351-2352.

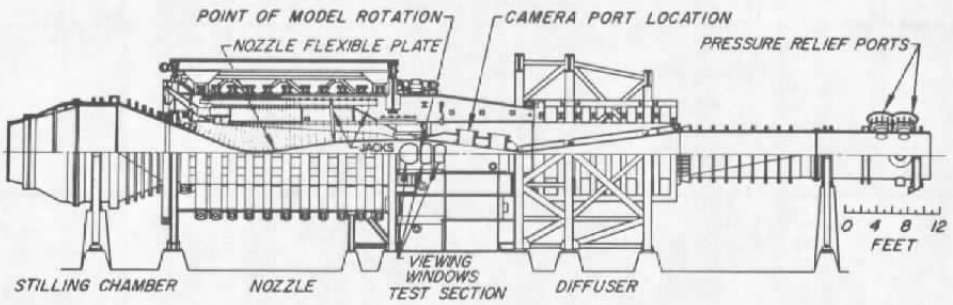

Assembly

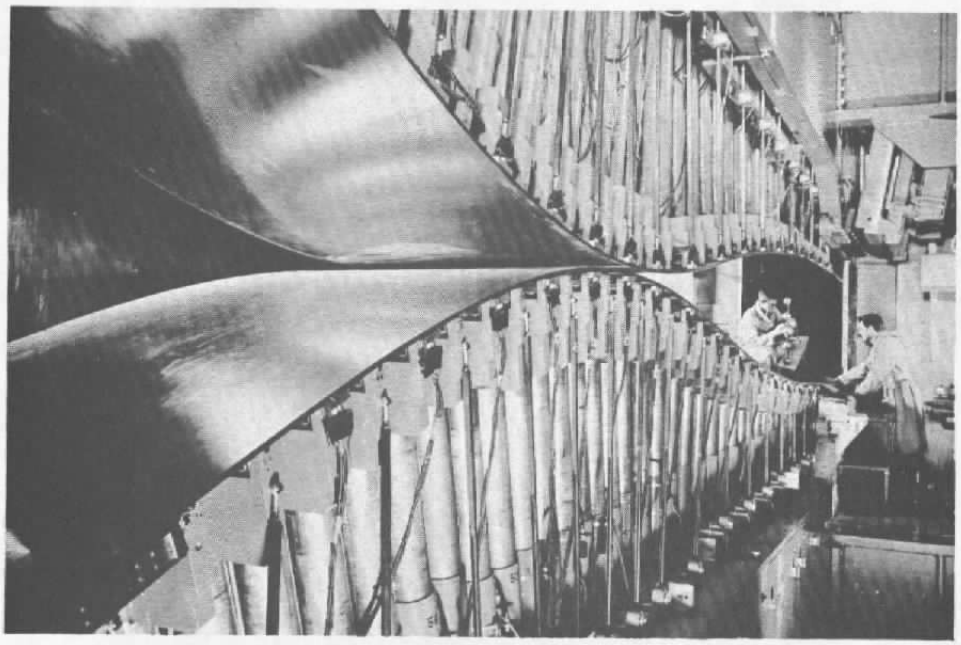

Nozzle and Test Section

a. Tunnel A

Fig. 1 Wind Tunnels

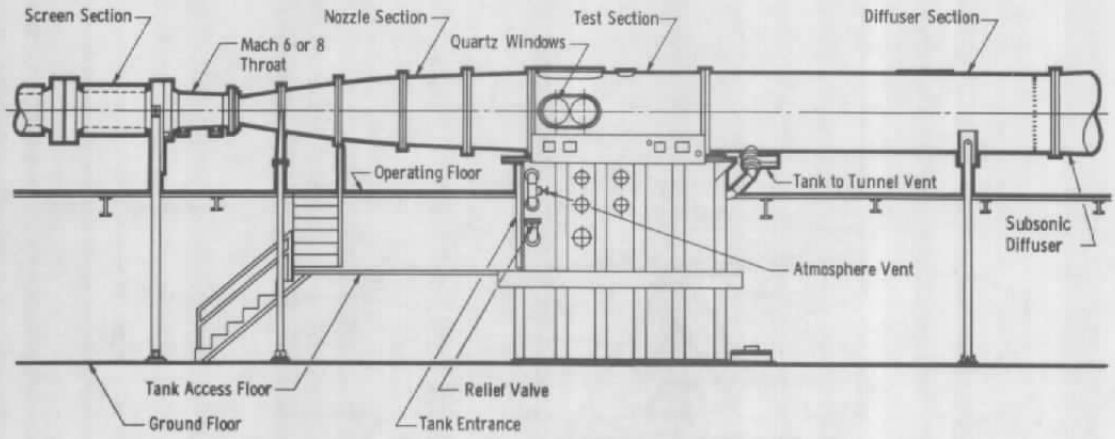

Tunnel Assembly

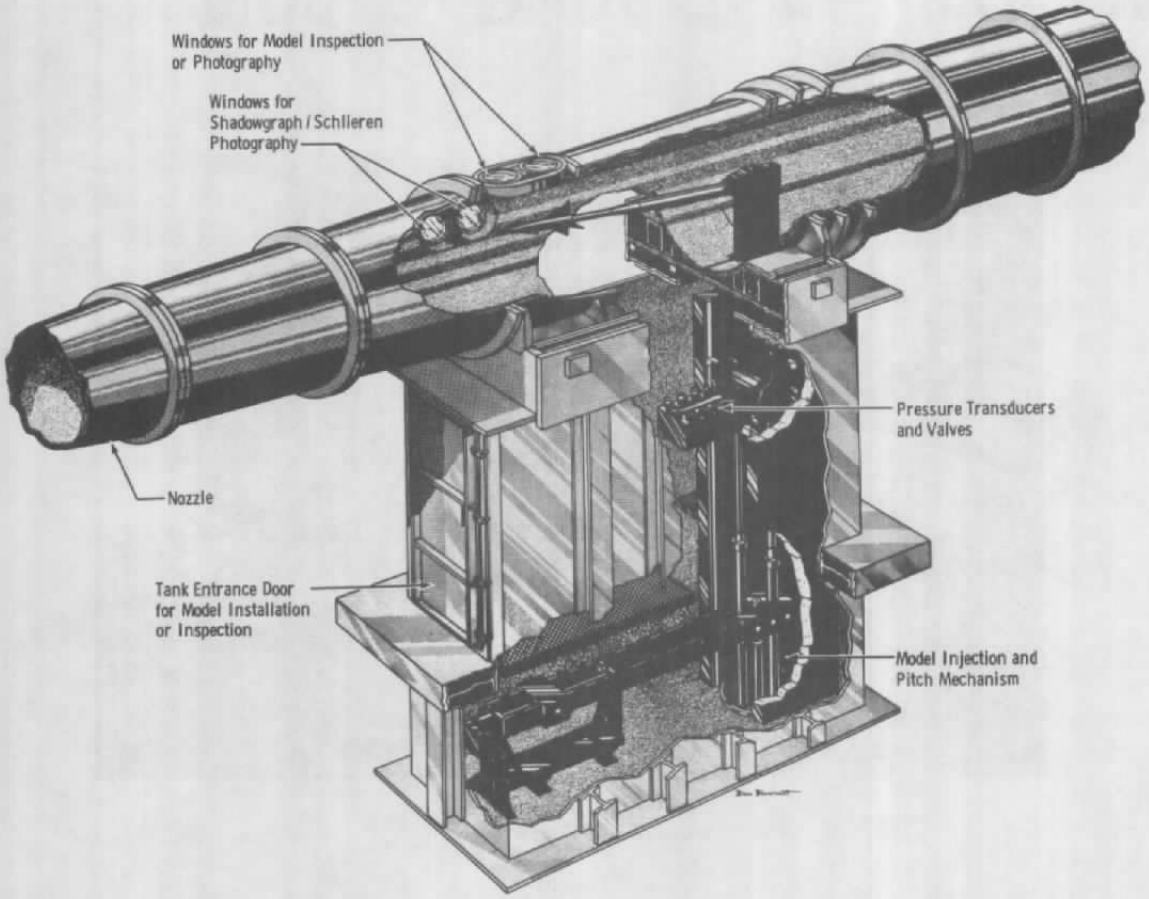

Tunnel Test Section

b. Tunnel B

Fig. 1 Continued

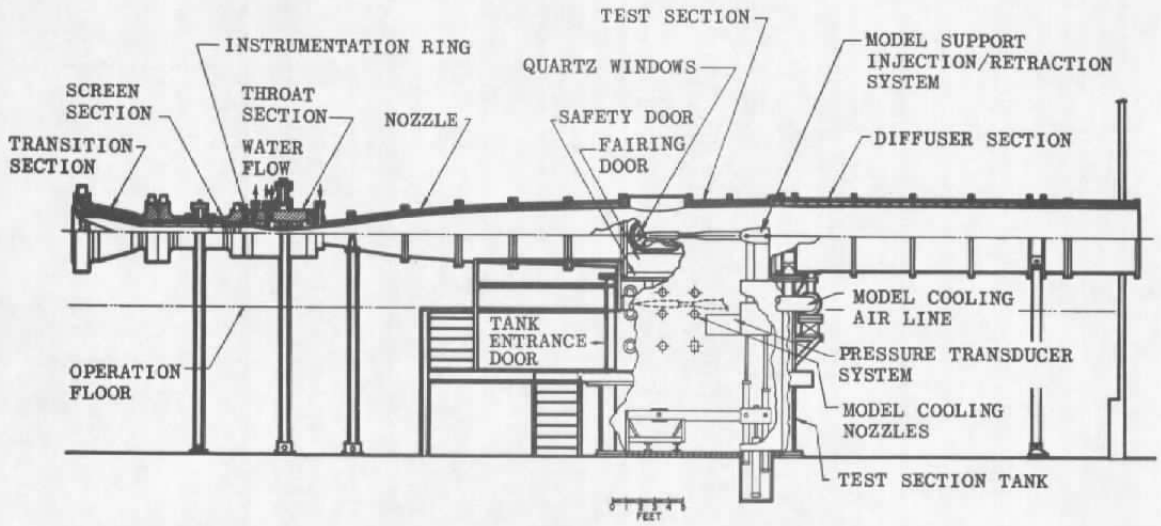

Tunnel Assembly

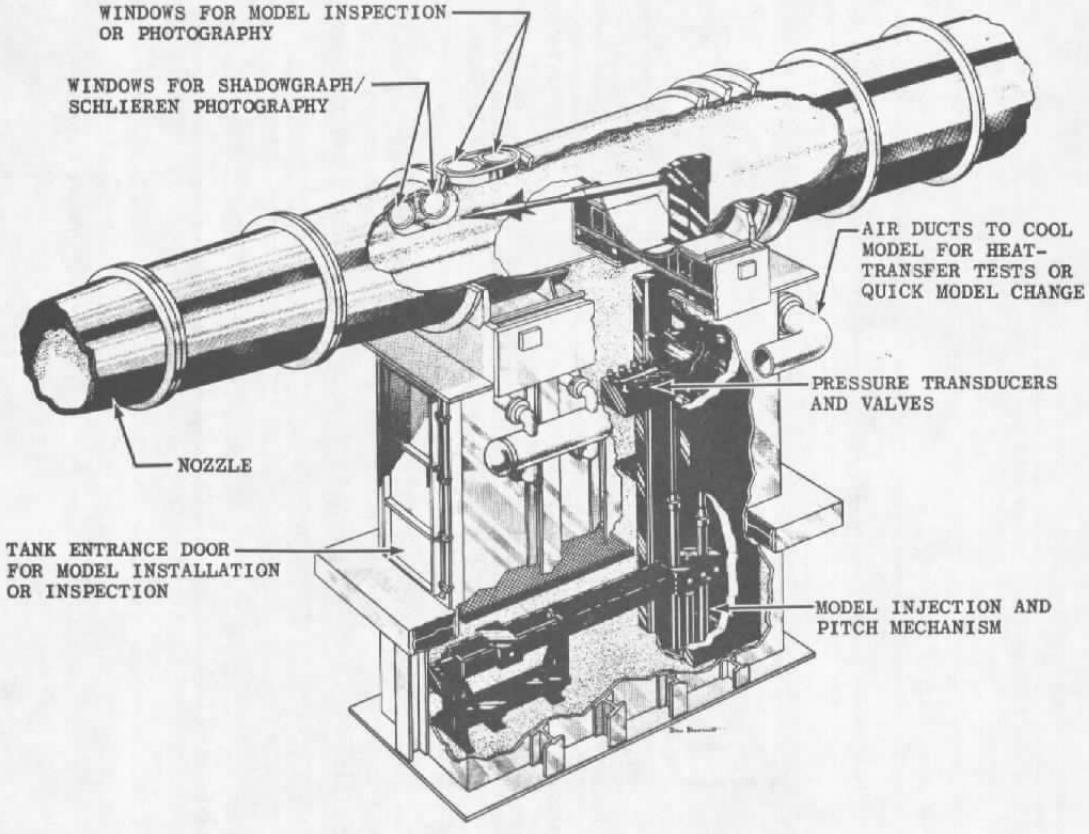

Tunnel Test Section

c. Tunnel C

Fig. 1 Concluded

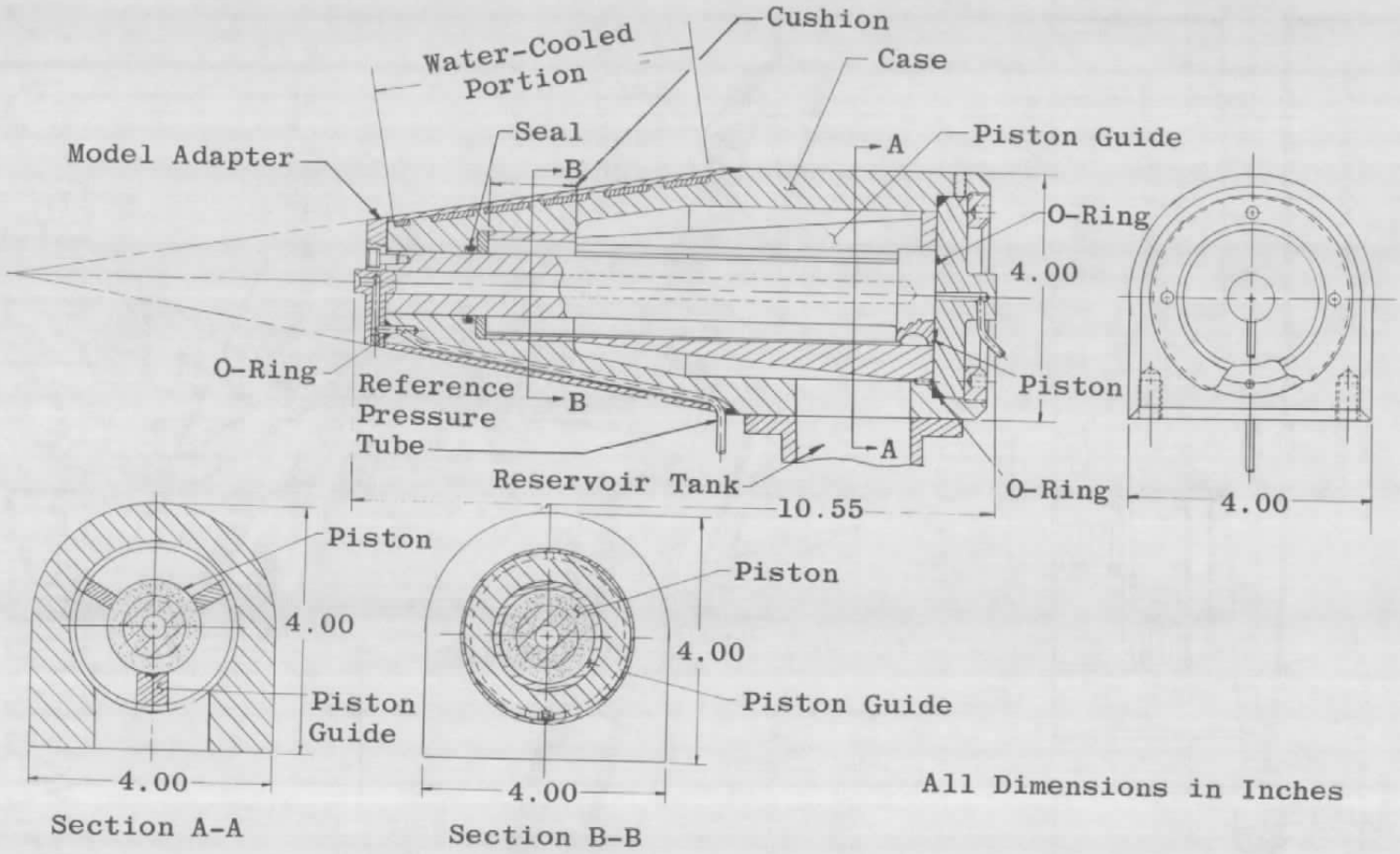

Fig. 2 Model Launcher

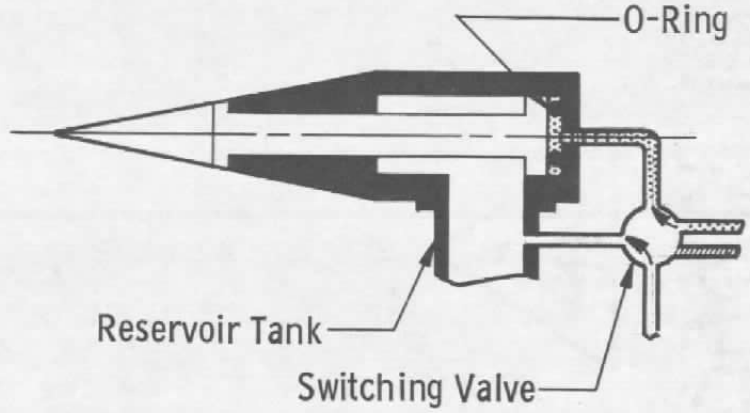

a. Charging

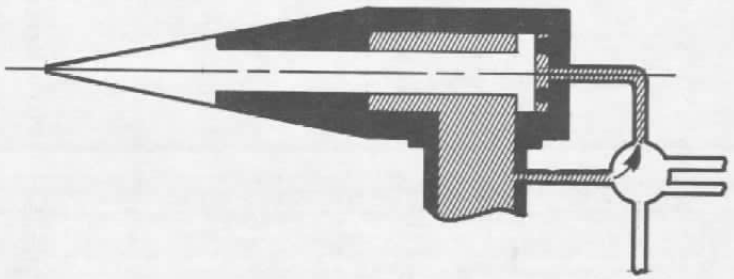

c. Firing

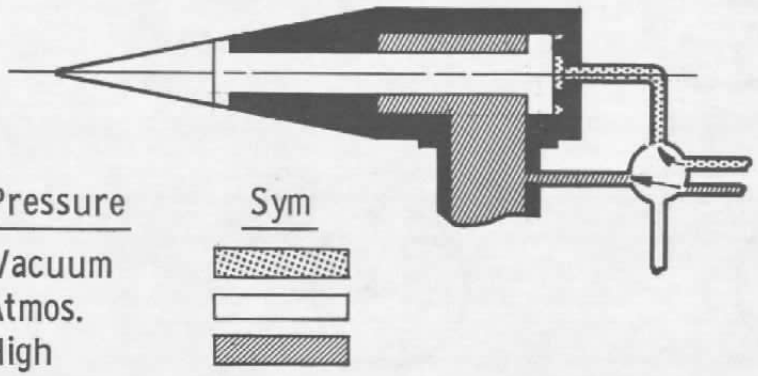

b. Charged

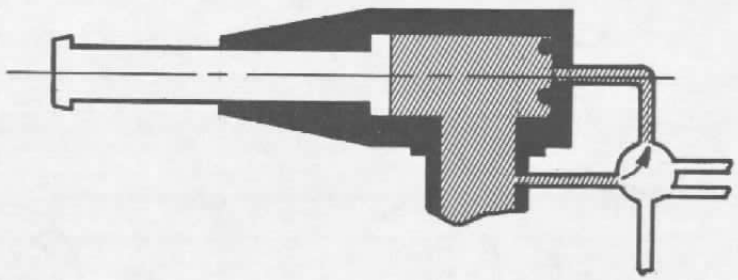

d. Launch

Fig. 3 Launcher Operation

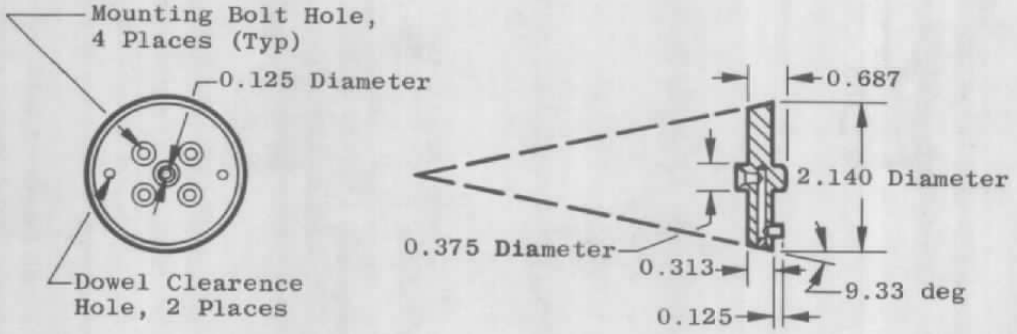

a. Pressure Model Adapter

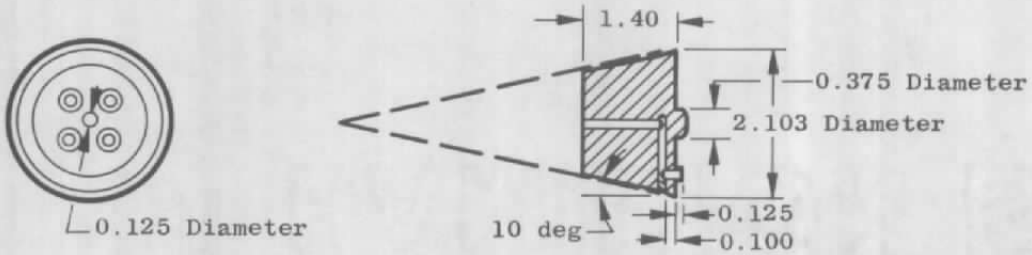

b. Drag Model Adapter

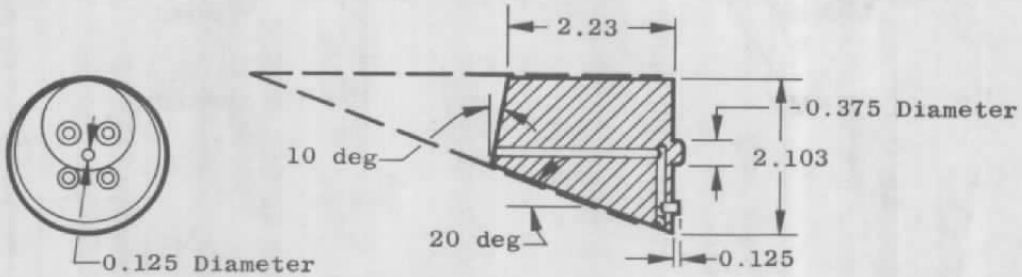

c. Moment Model Adapter

Fig. 4 Model Adapters

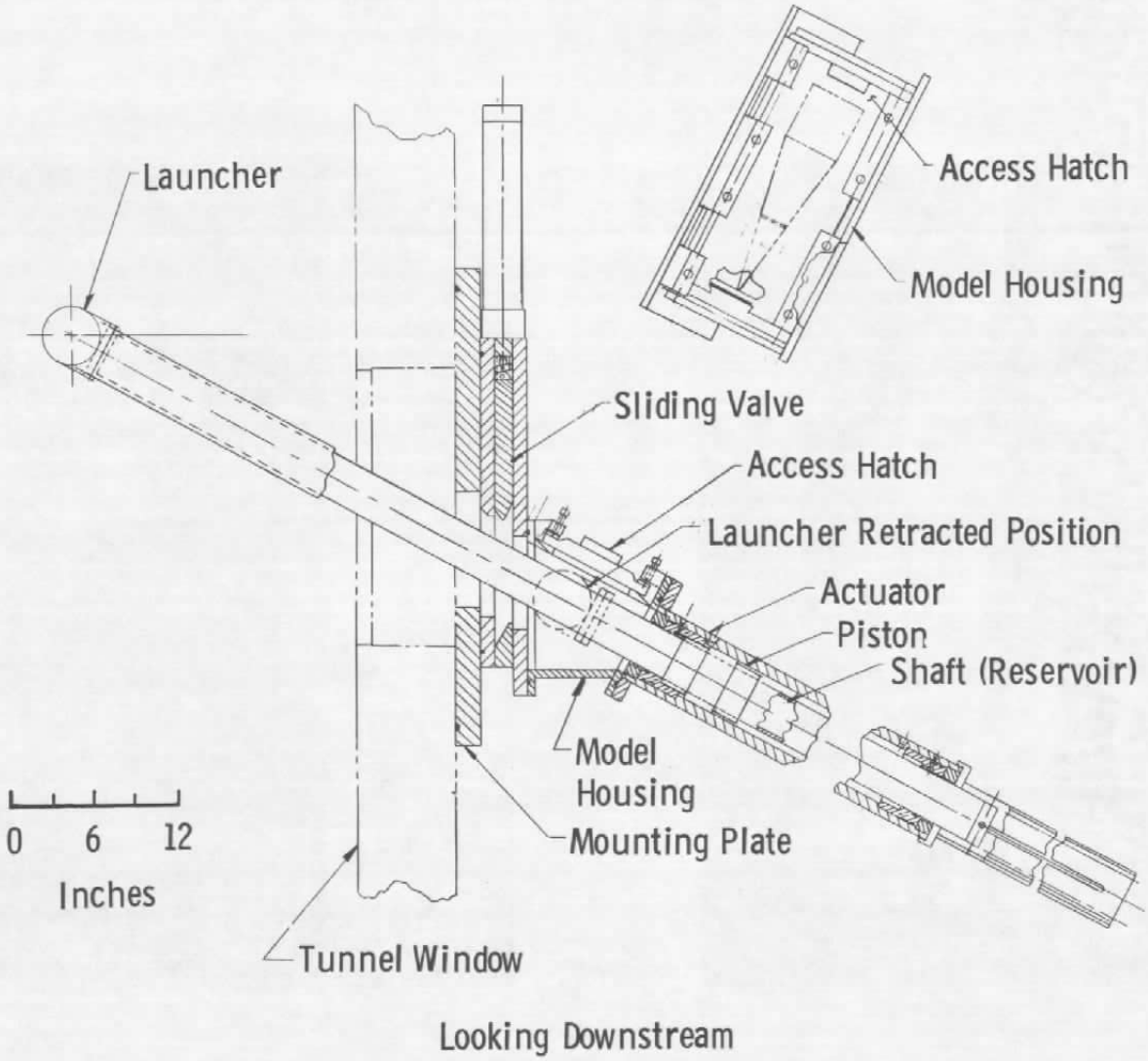

Fig. 5 Tunnel A Launcher Support System

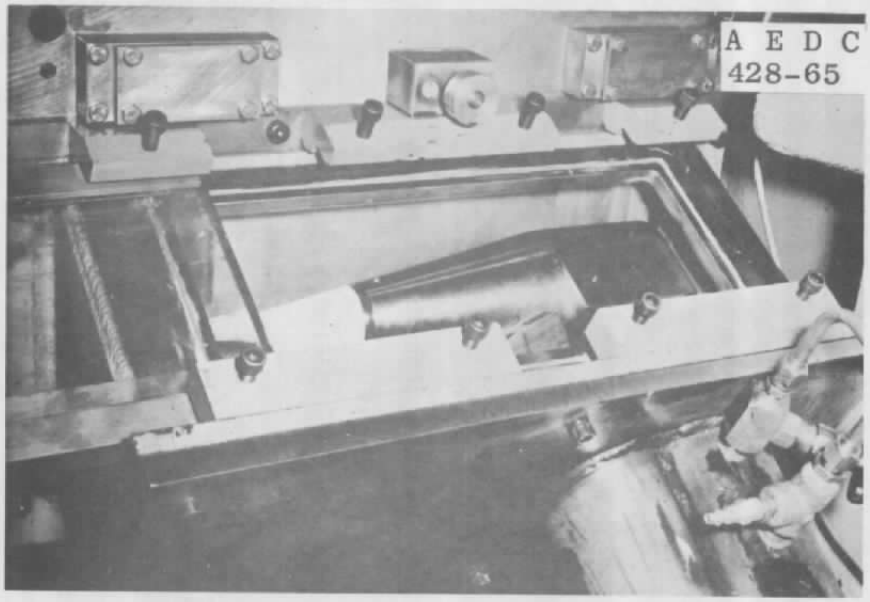

Fig. 6 Model Housing (Hatch Open)

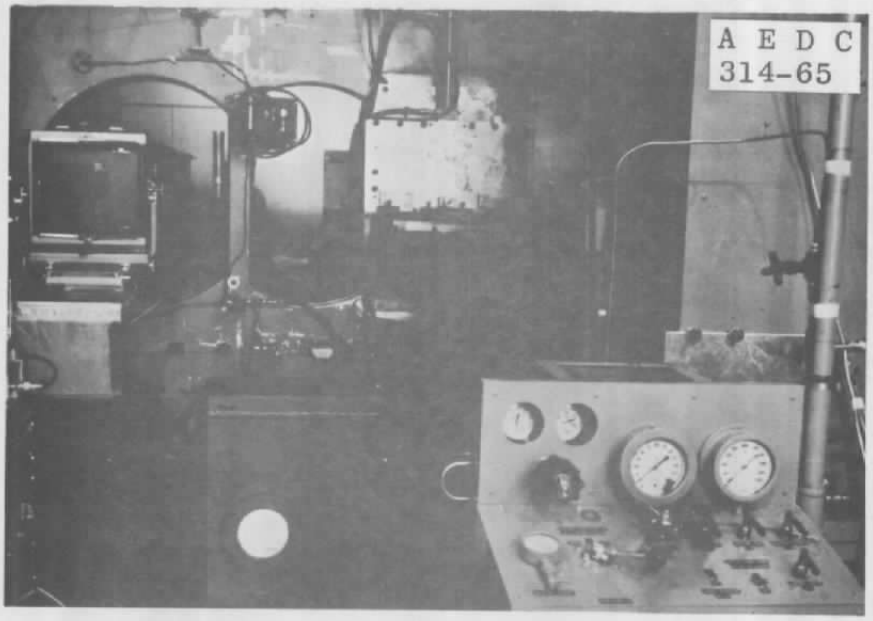

Fig. 7 System Installed on Tunnel A

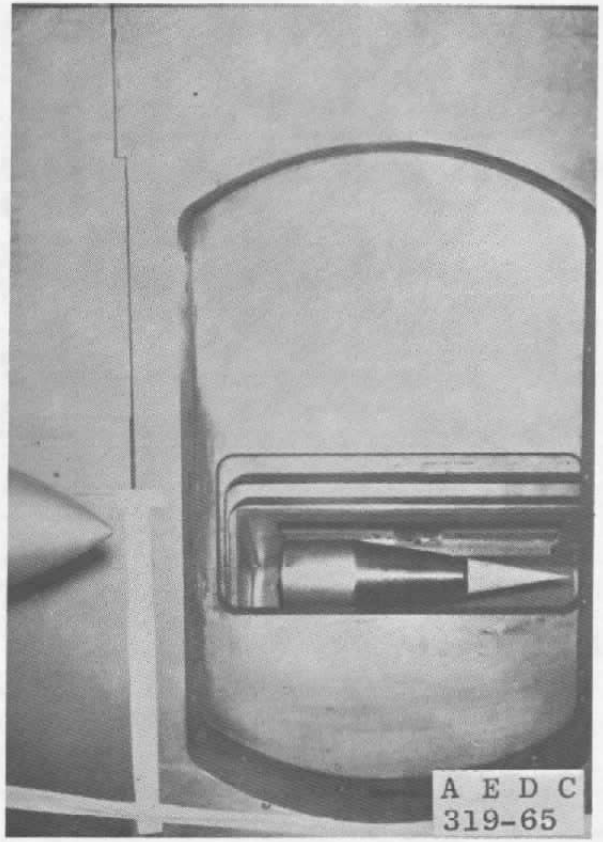

a. System Retracted

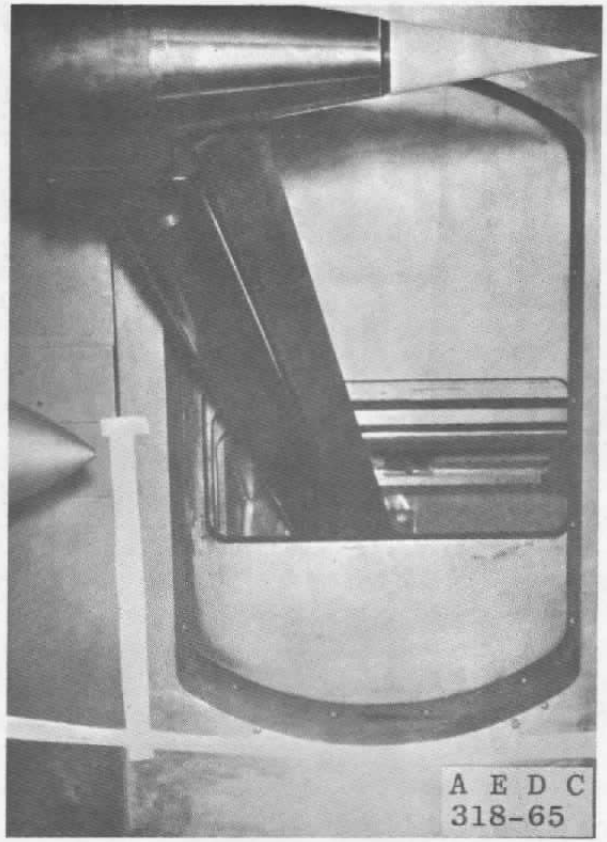

b. System Injected

Fig. 8 Operation of the Tunnel A Model Launcher System

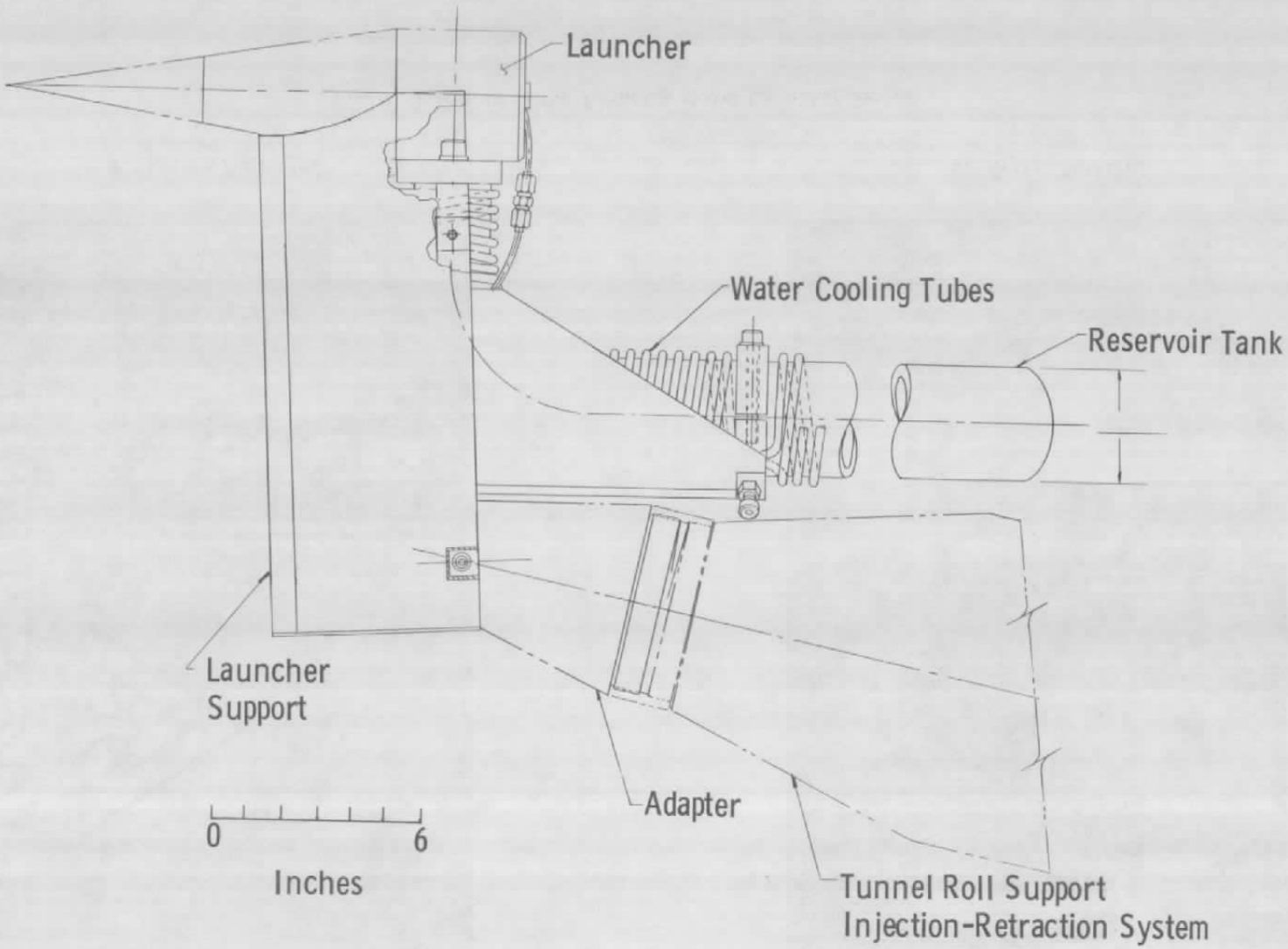

Fig. 9 Tunnel B and C Launcher Support System

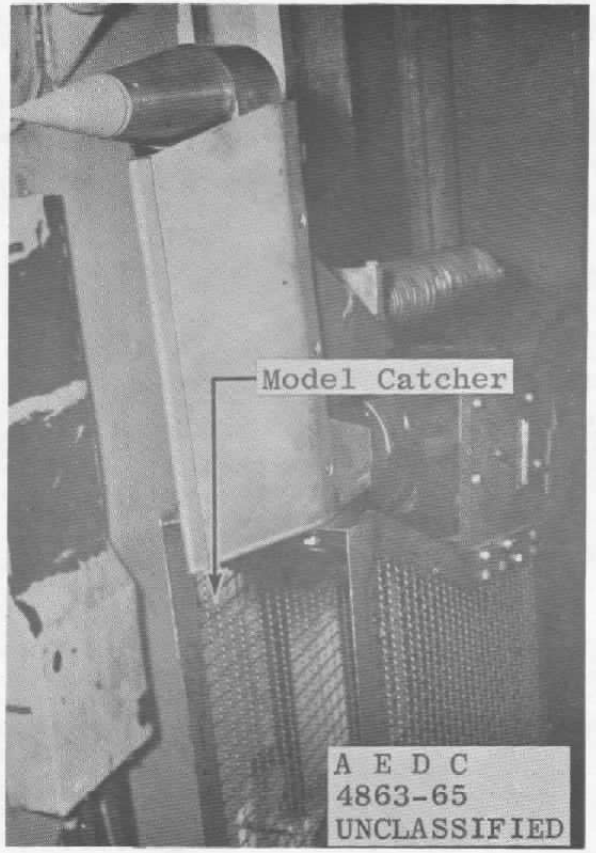

a. System Retracted

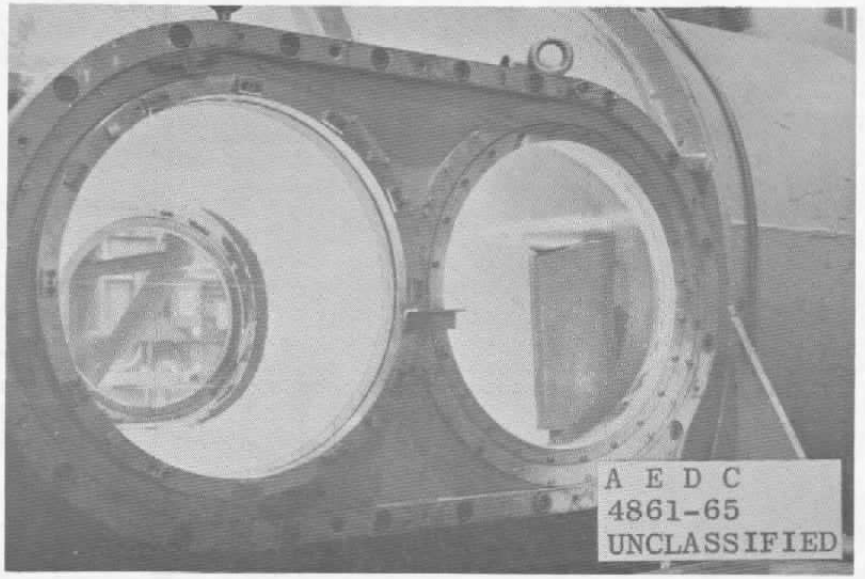

b. System Injected

Fig. 10 Operation of the Tunnel B and C Model Launcher System

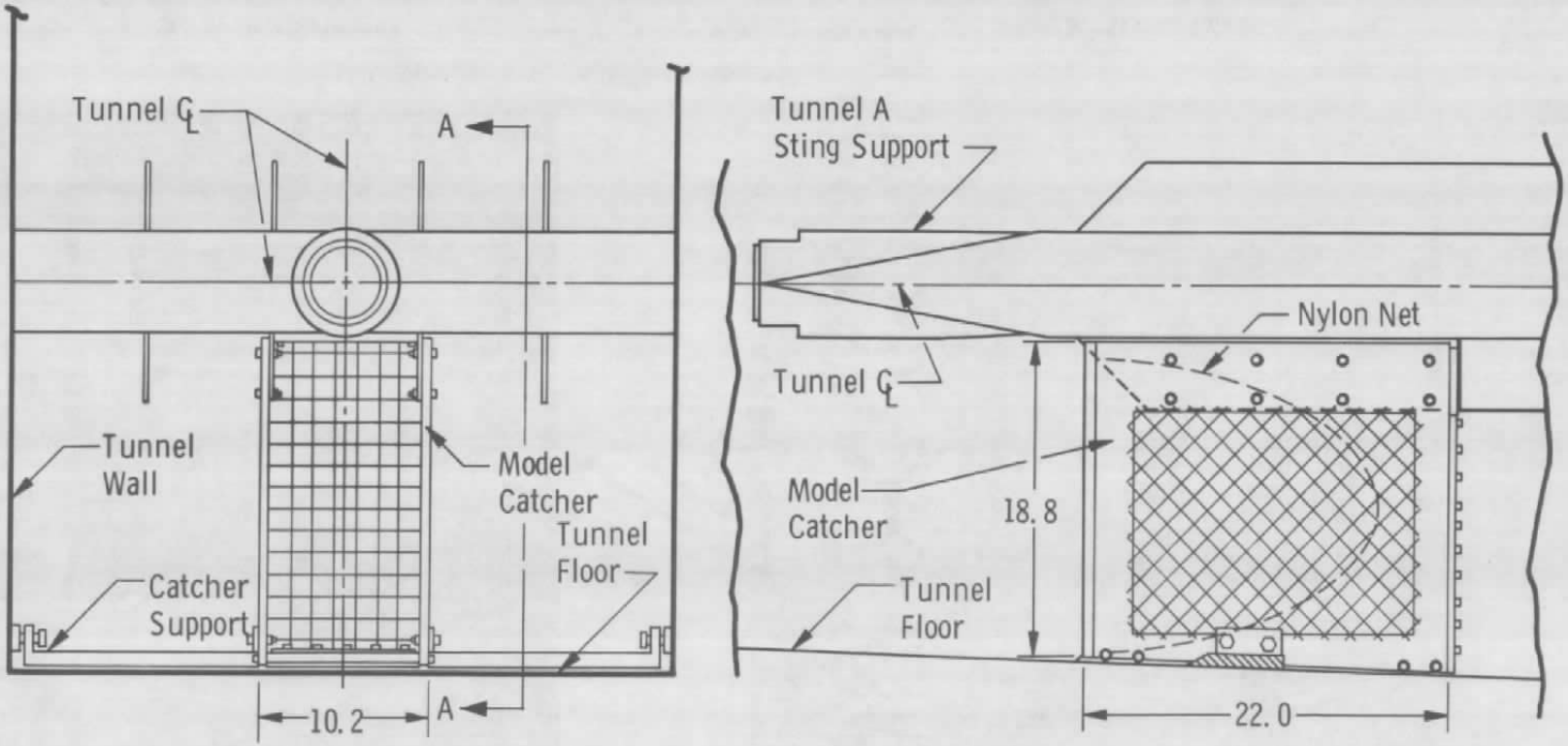

Section A-A

All Dimensions in Inches

Fig. 11 Tunnel A Model Catcher Installation

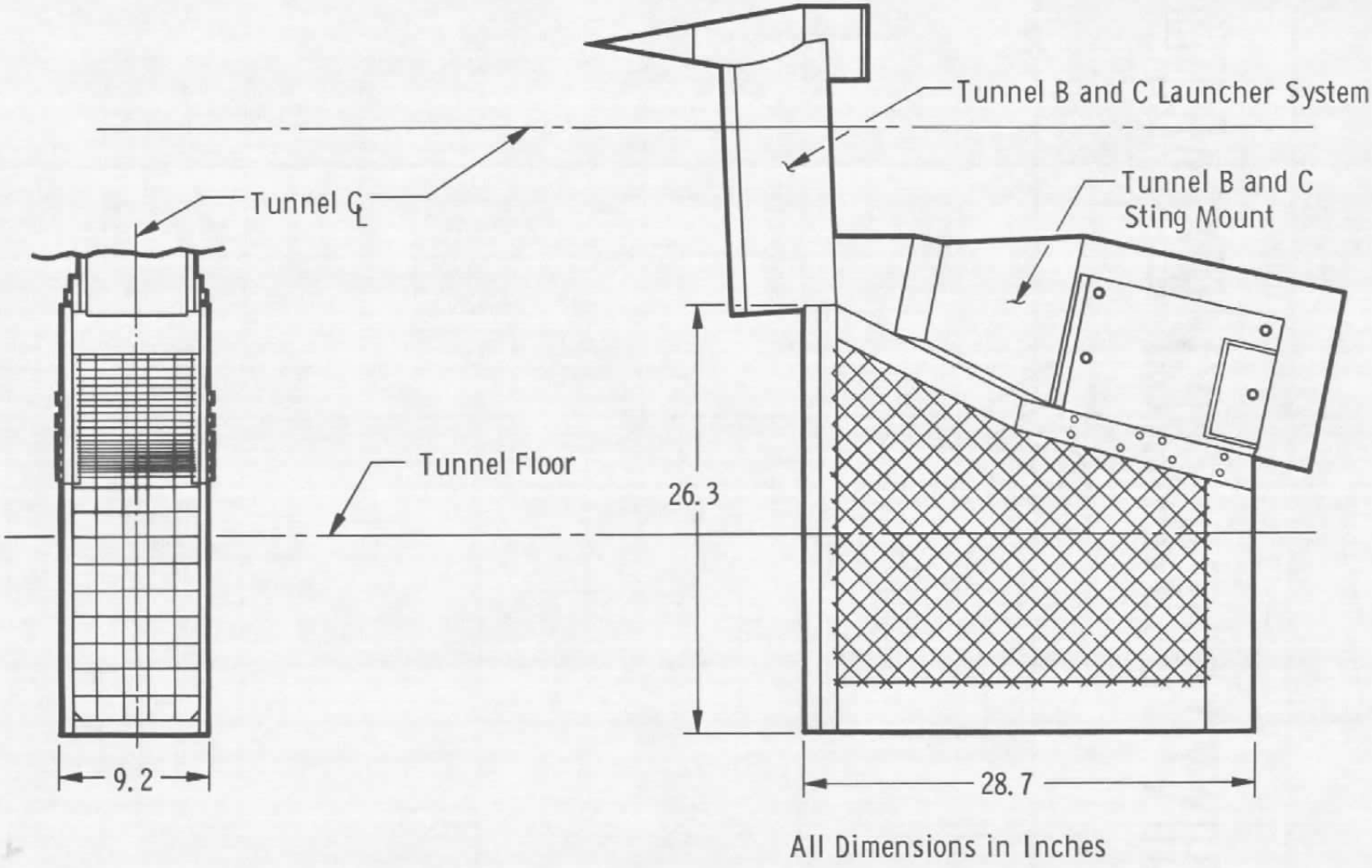

Fig. 12 Tunnel B and C Model Catcher Installation

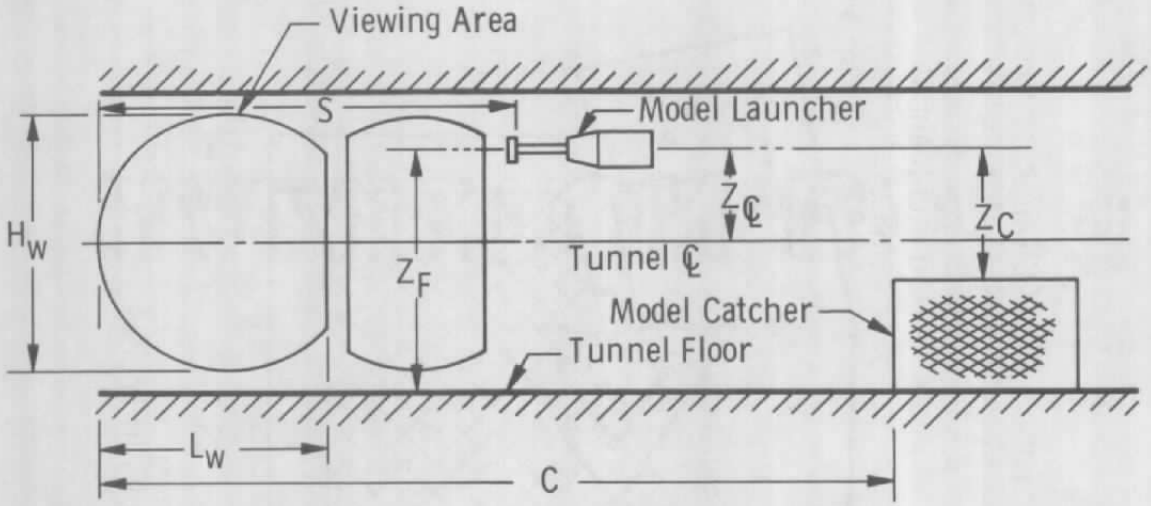

Tunnel A

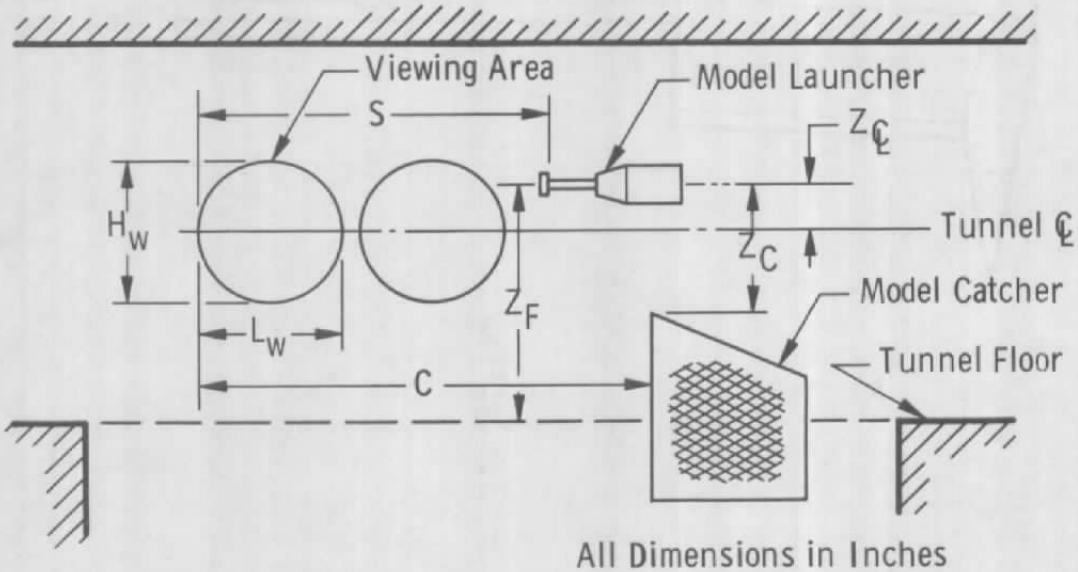

All Dimensions in Inches

Tunnels B and C

Tunnel	C	H_W	L_W	S	Z_C	$Z_{℄}$	Z_F
A	104.2	34.0	29.2	54.6	15.6	12.6	32.6
B and C	58.7	17.8	17.8	45.5	17.5	6.0	45.5

Fig. 13 Trajectory Parameters

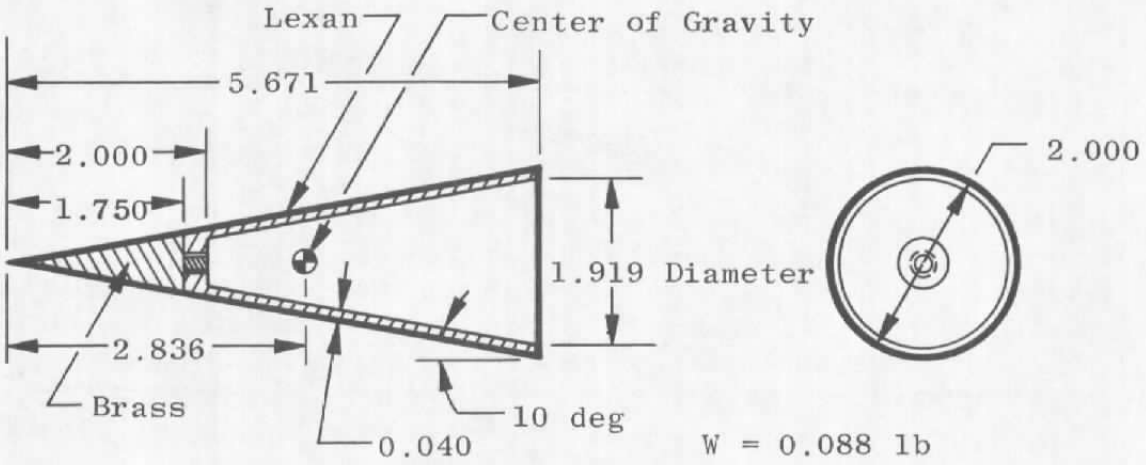

a. Supersonic Drag Model

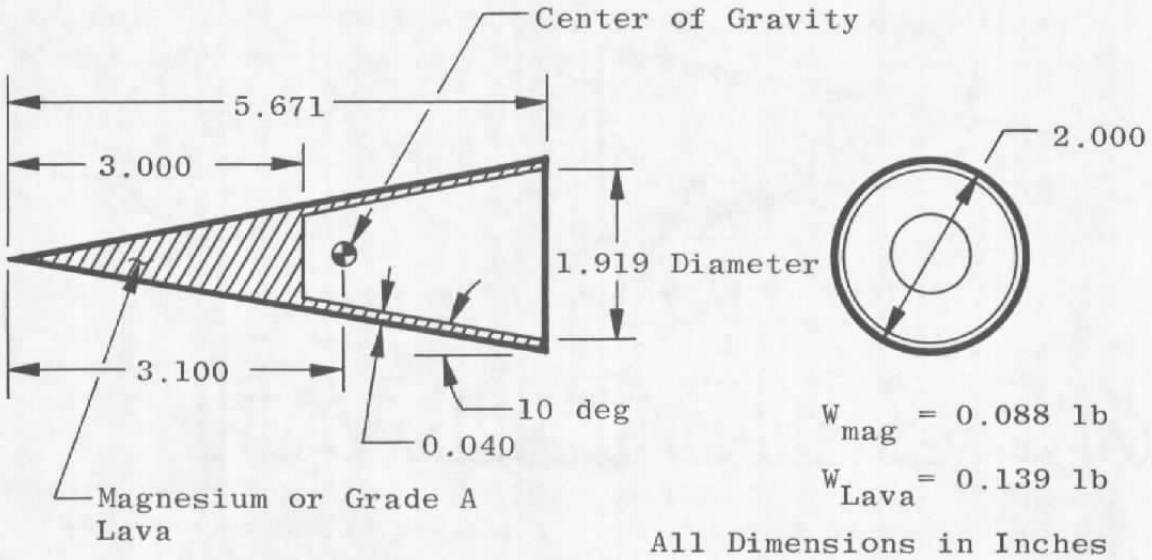

b. Hypersonic Drag Model

Fig. 14 Drag Models

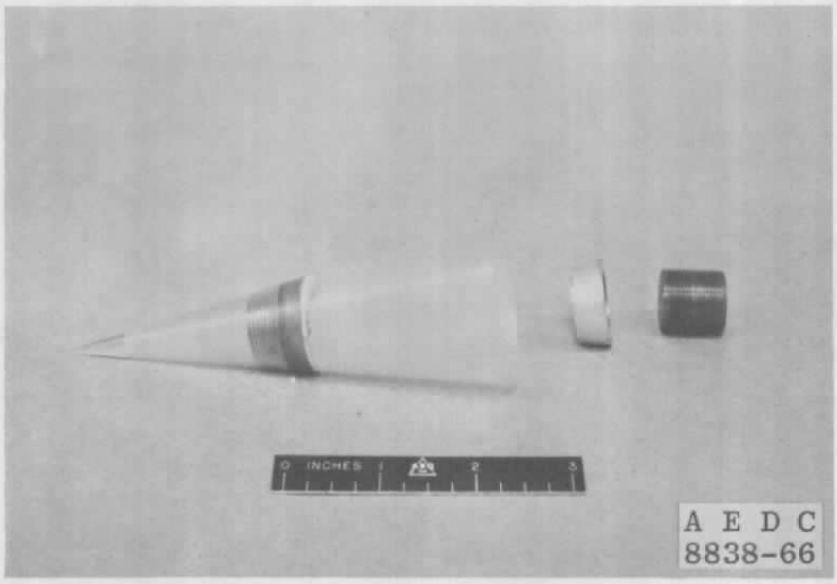

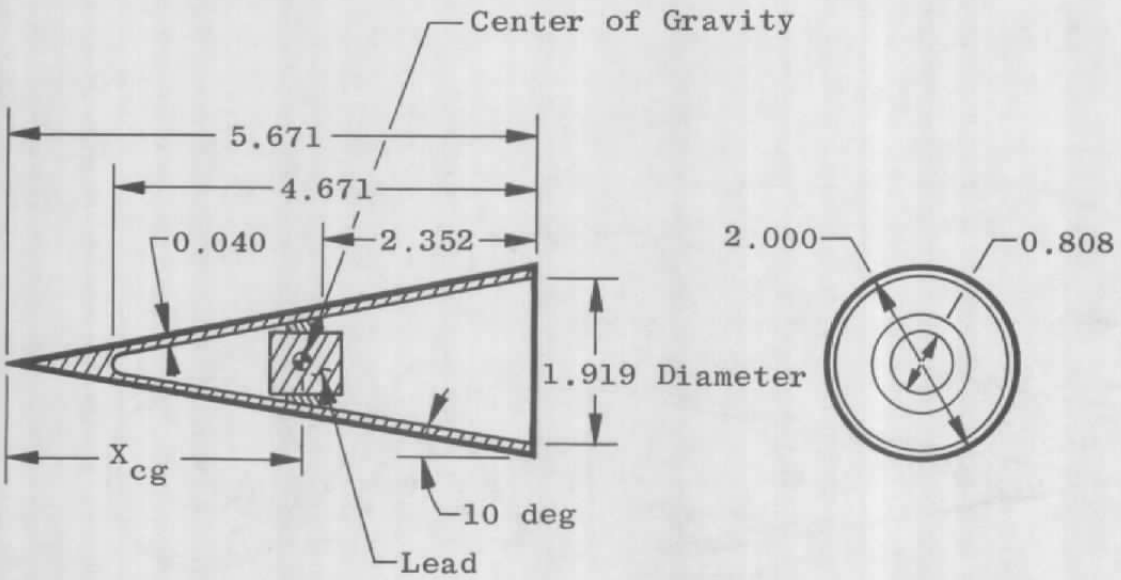

Material	W, lb	X_{cg}	I x 10^5, slug-ft^2
Lexan	0.192	3.119	2.633
Magnesium	0.208	3.119	2.863
Lava	0.238	3.173	5.051

All Dimensions in Inches

Fig. 15 Moment Model

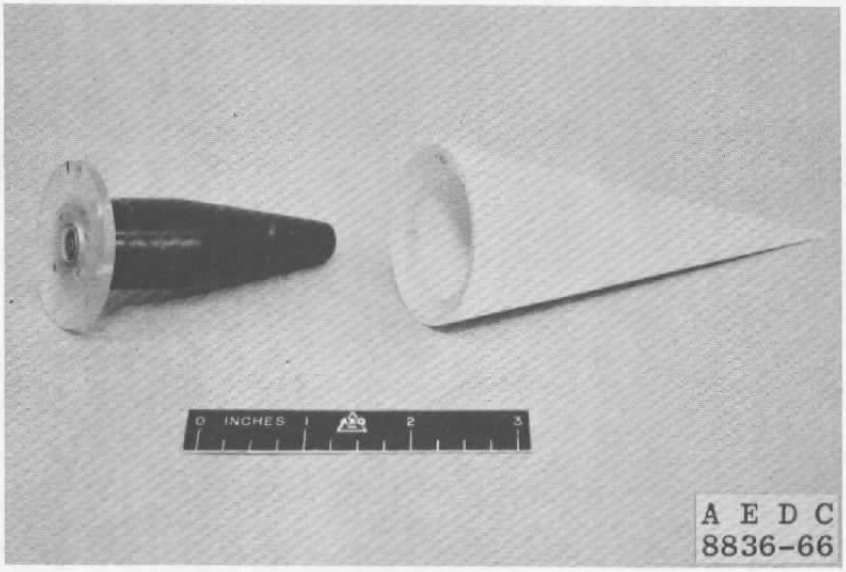

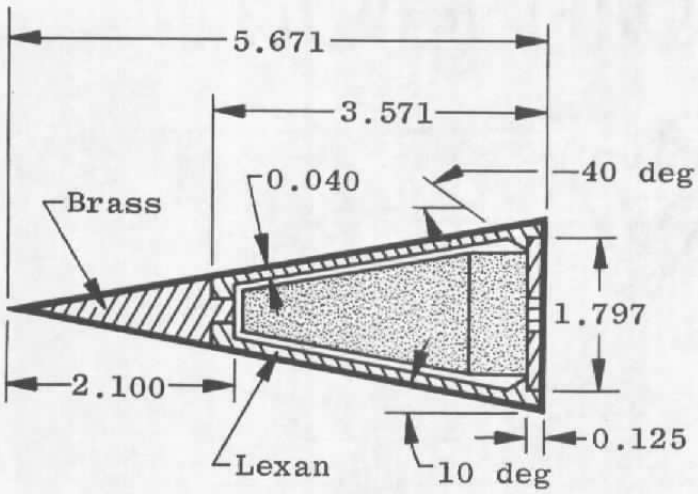

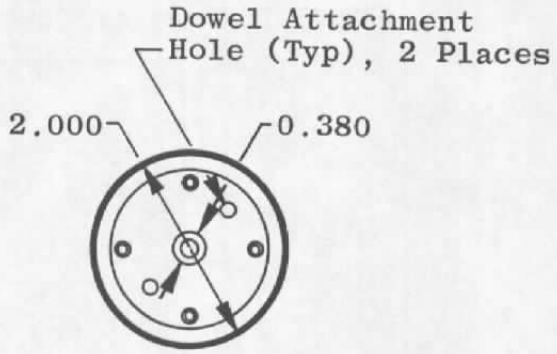

W_{model} = 0.139 lb

W_{total} = 0.262 lb

All Dimensions in Inches

Fig. 16 Pressure Telemetry Model

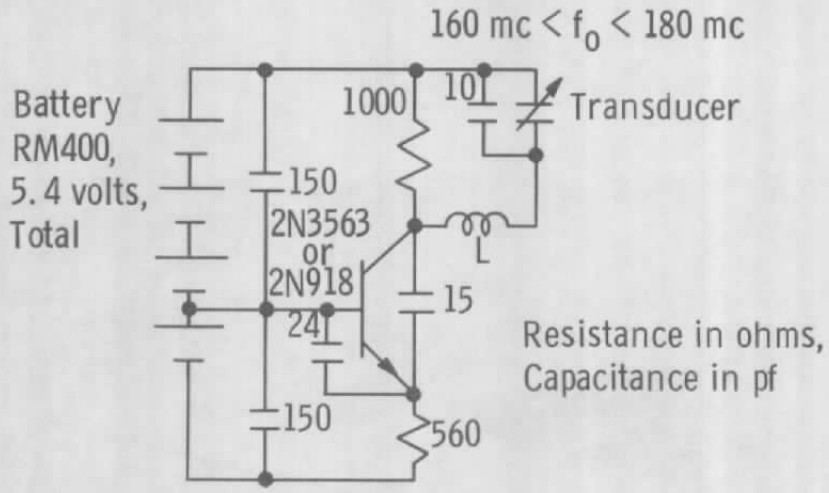

Fig. 17 Telemeter Circuit Diagram

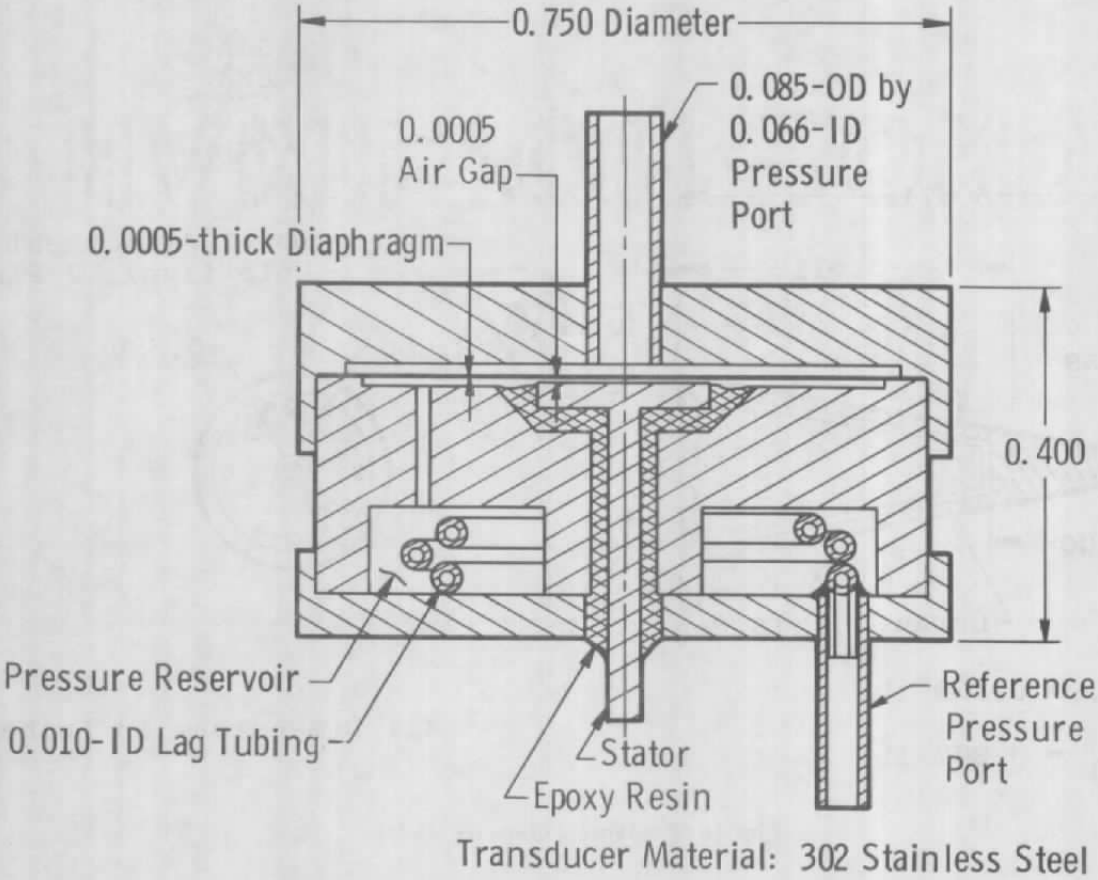

Fig. 18 Pressure Tranducer

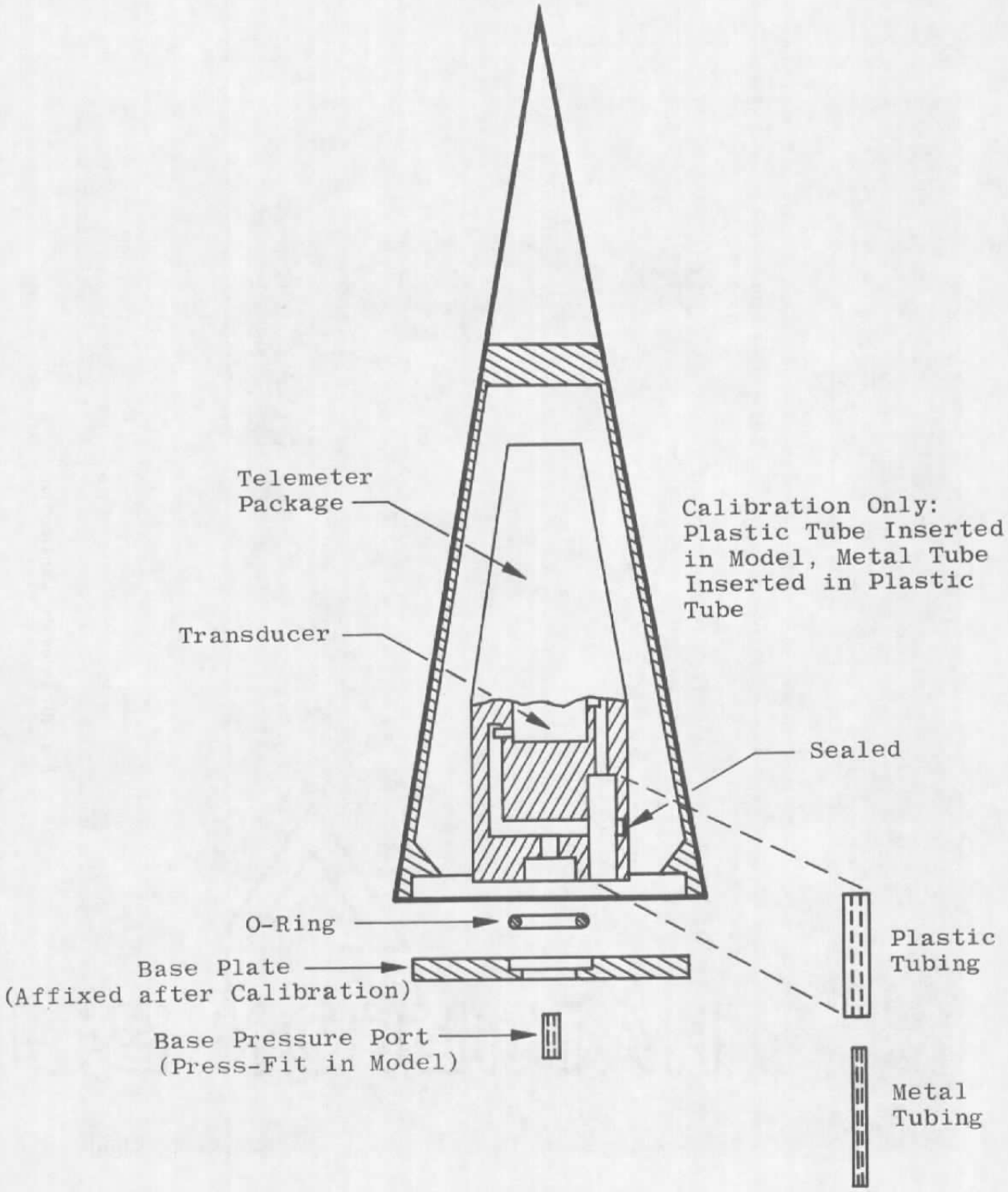

Fig. 19 Pressure Routing System

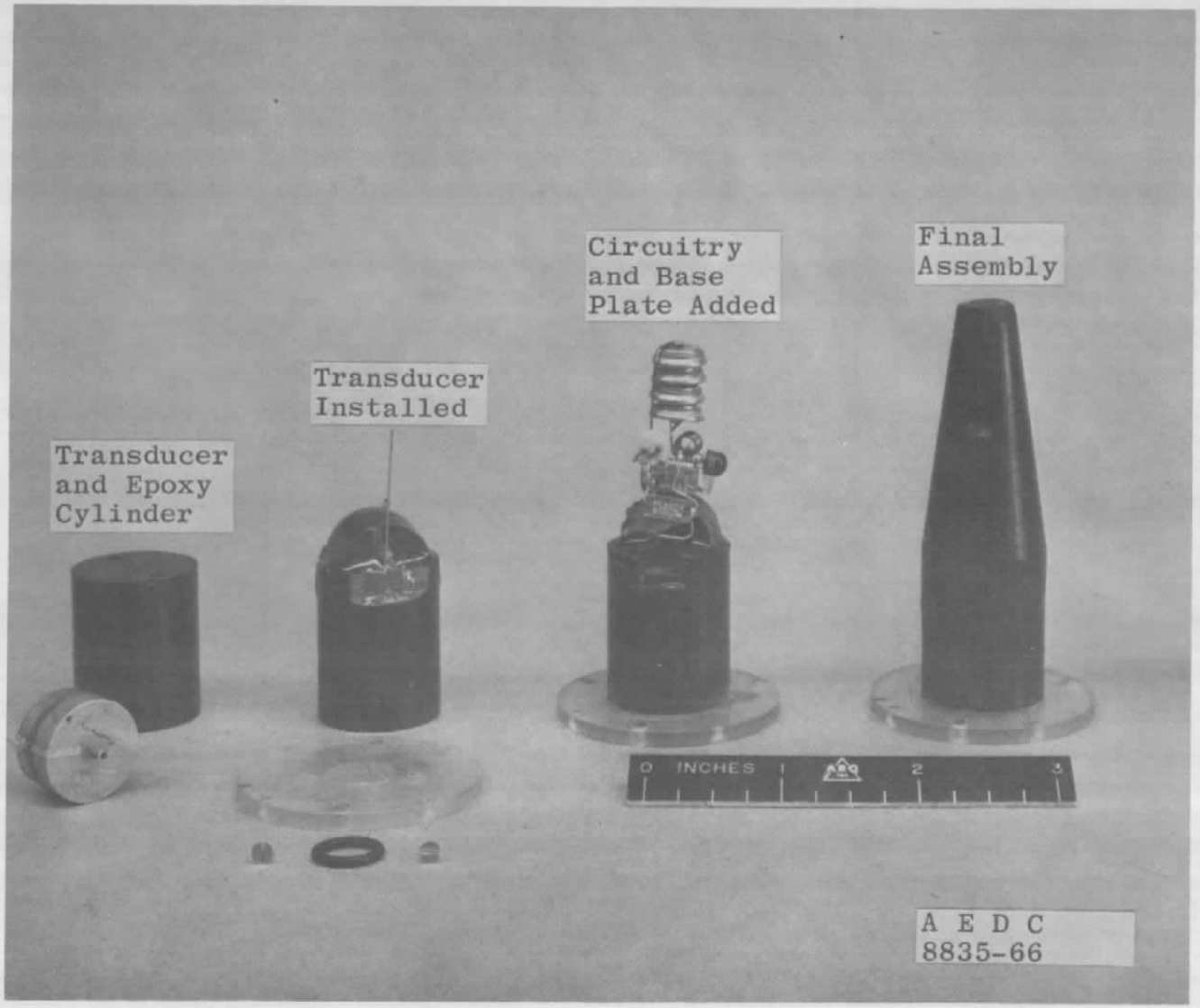

Fig. 20 Telemeter Construction

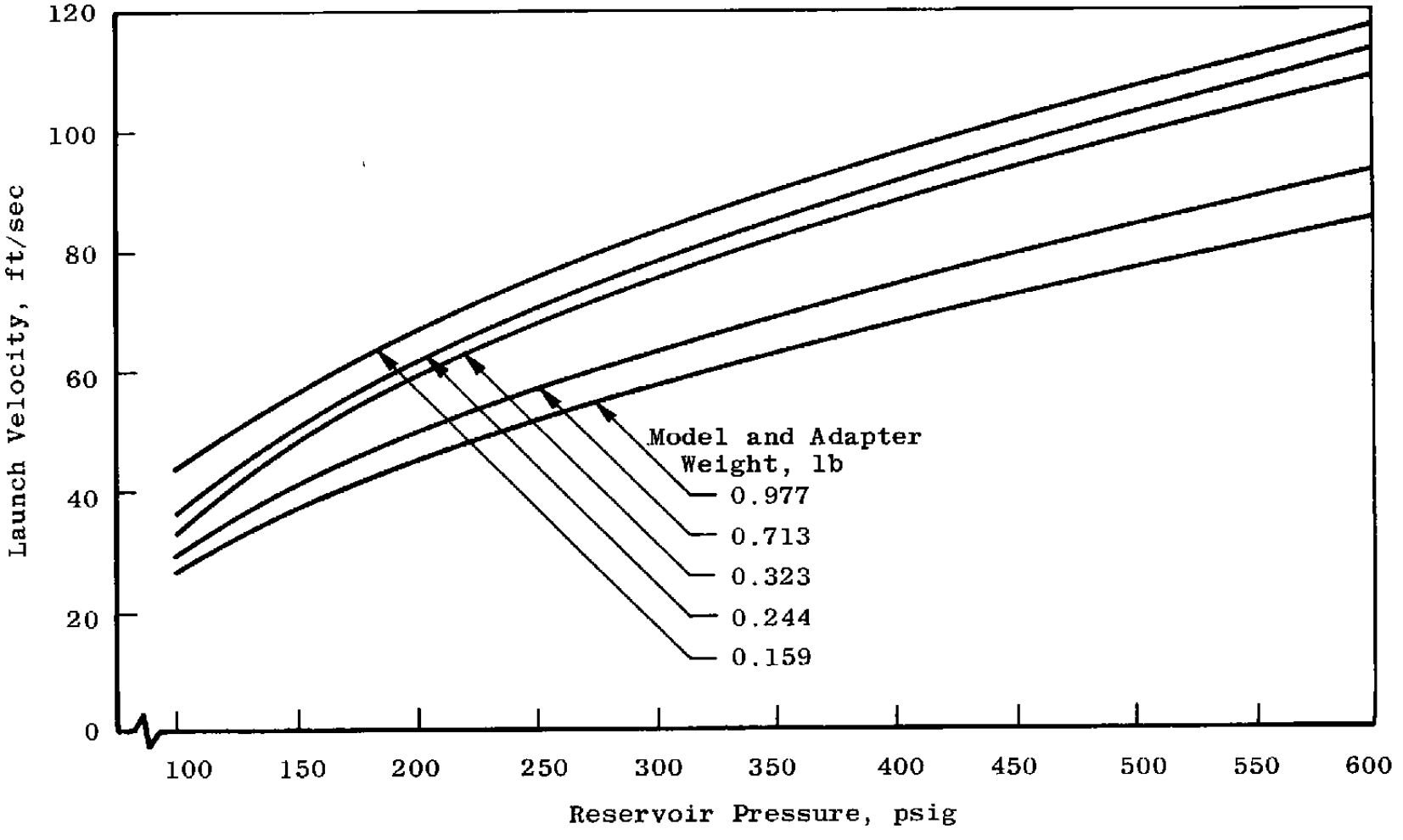

Fig. 21 Launcher Performance

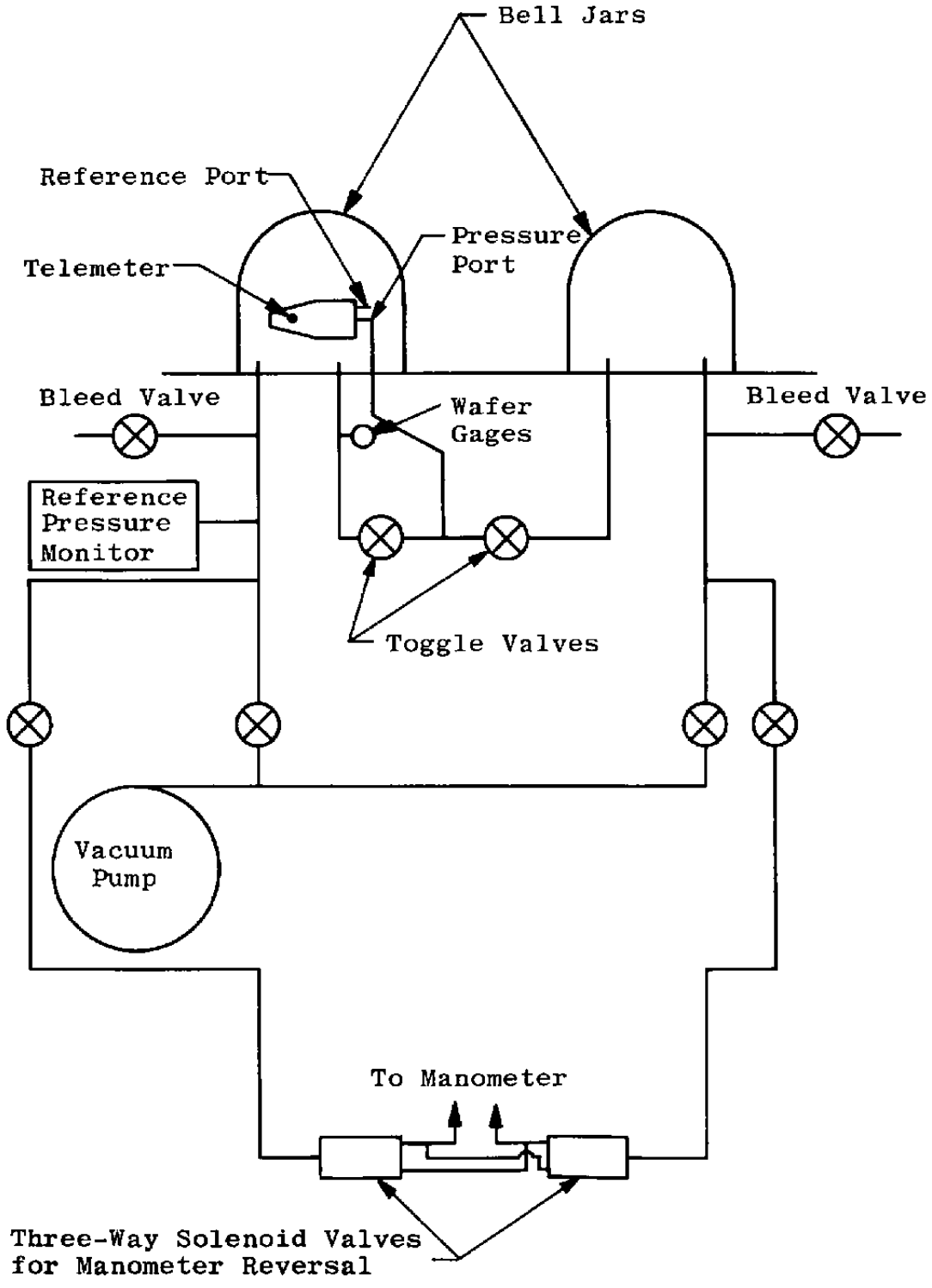

Fig. 22 Pressure Calibration Apparatus

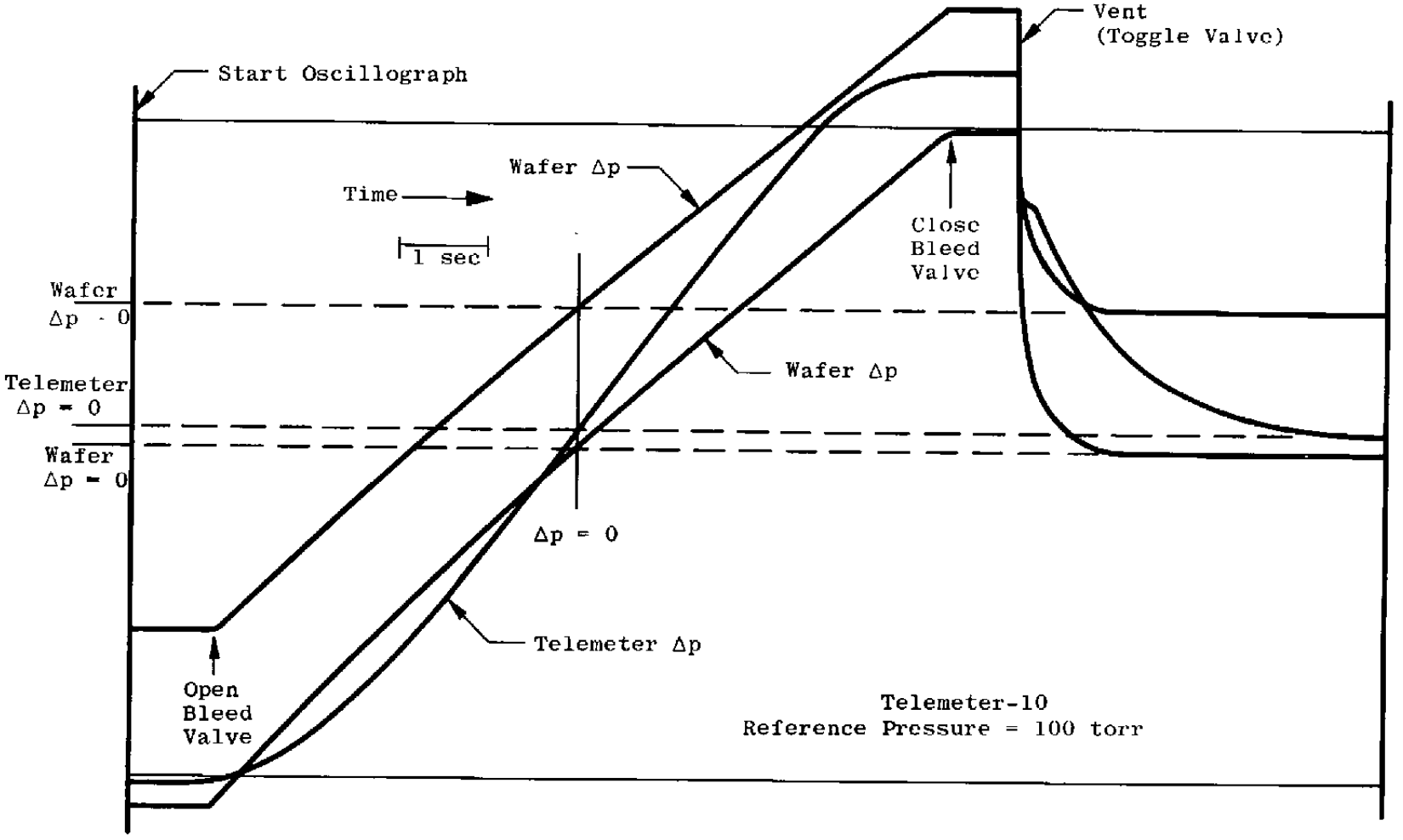

Fig. 23 Pressure Calibration Trace

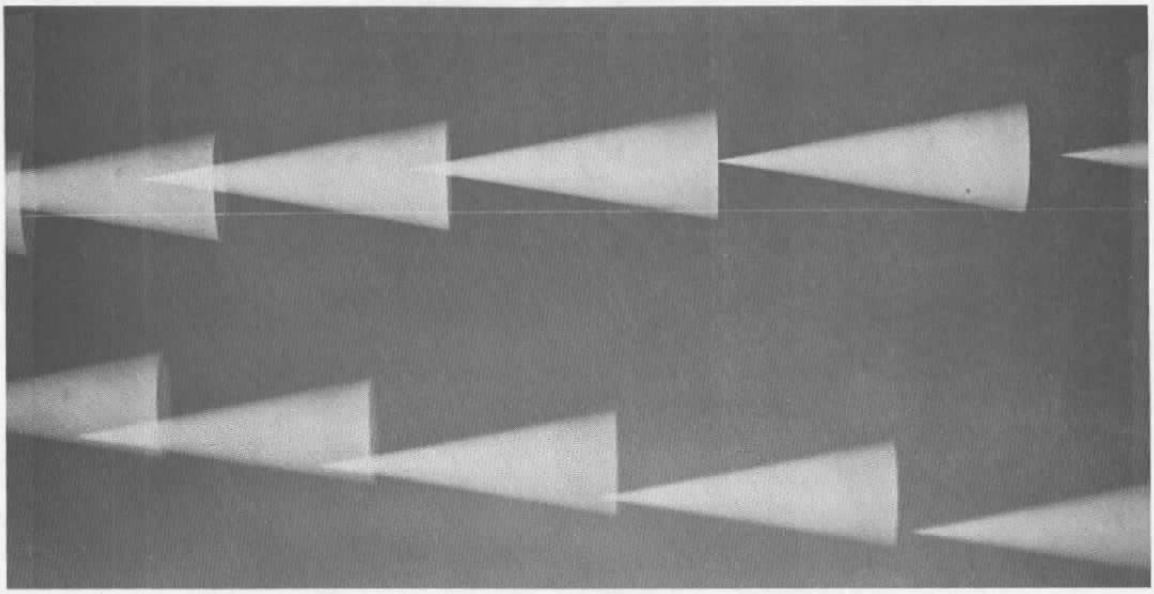

a. Nonoscillating Model

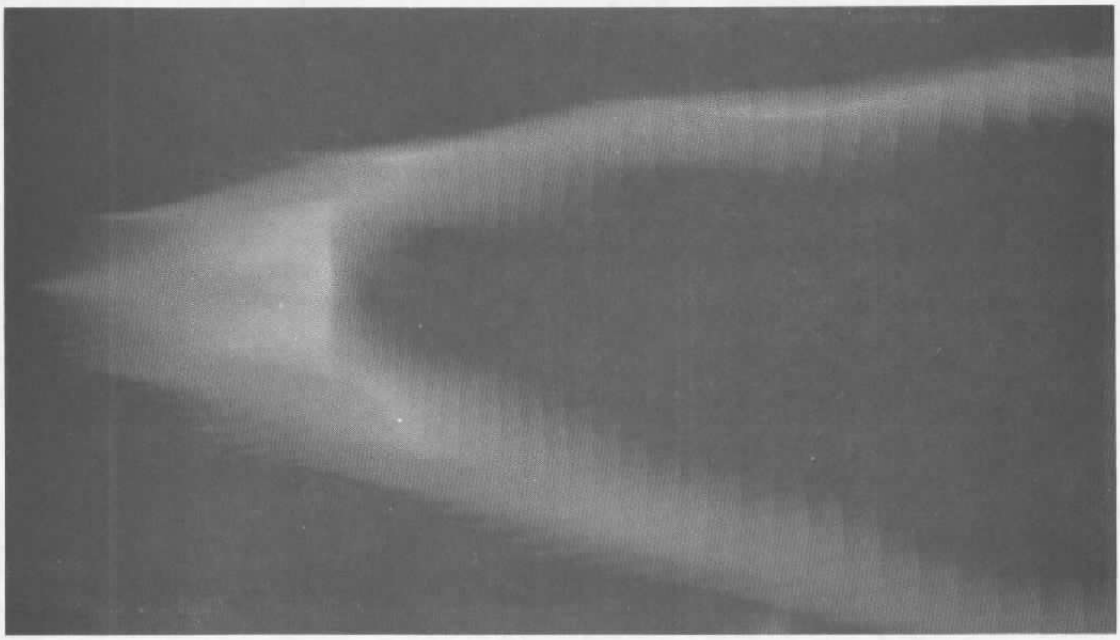

b. Oscillating Model

Fig. 24 Multi-Exposure Photographs

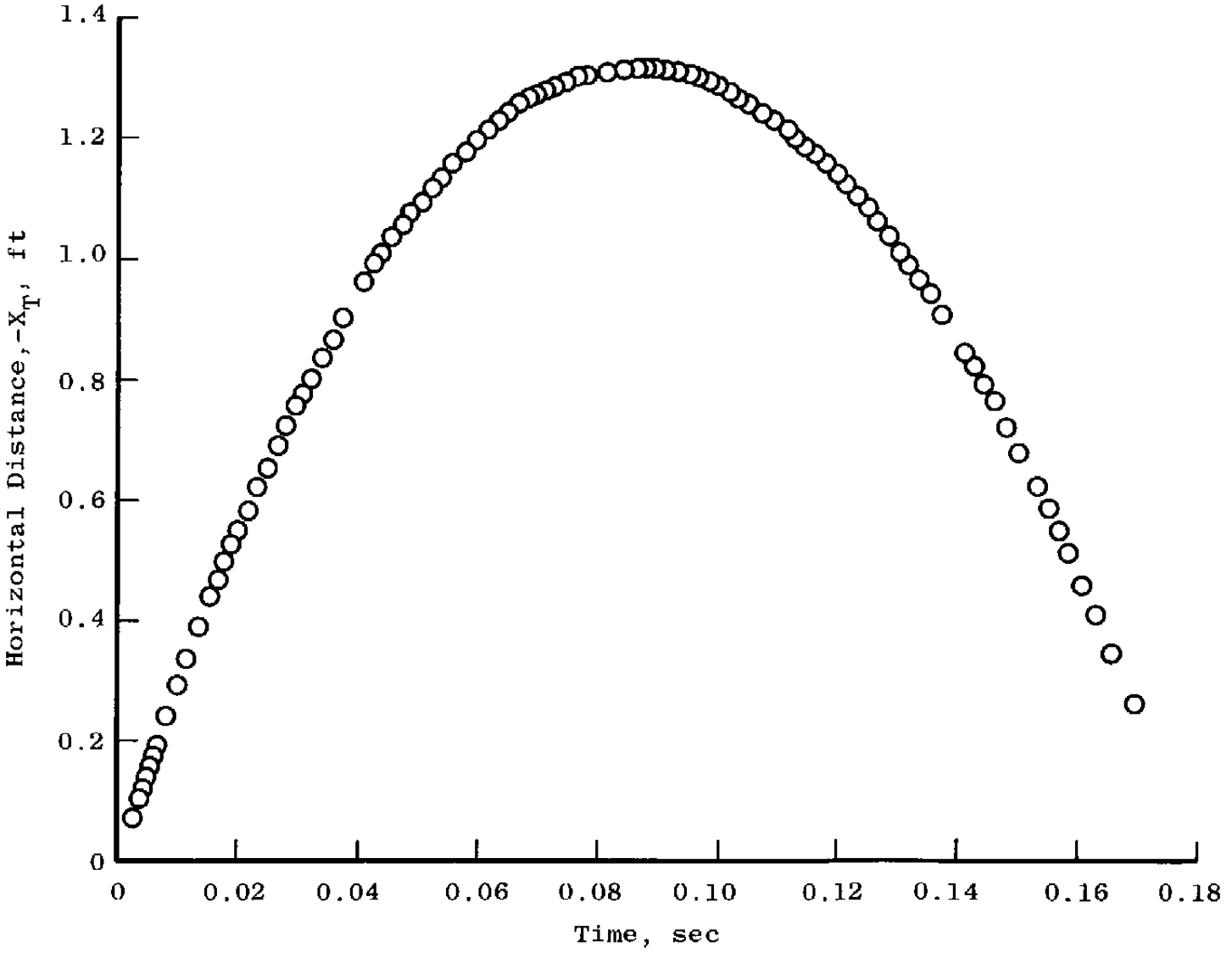

Fig. 25 Distance-Time History

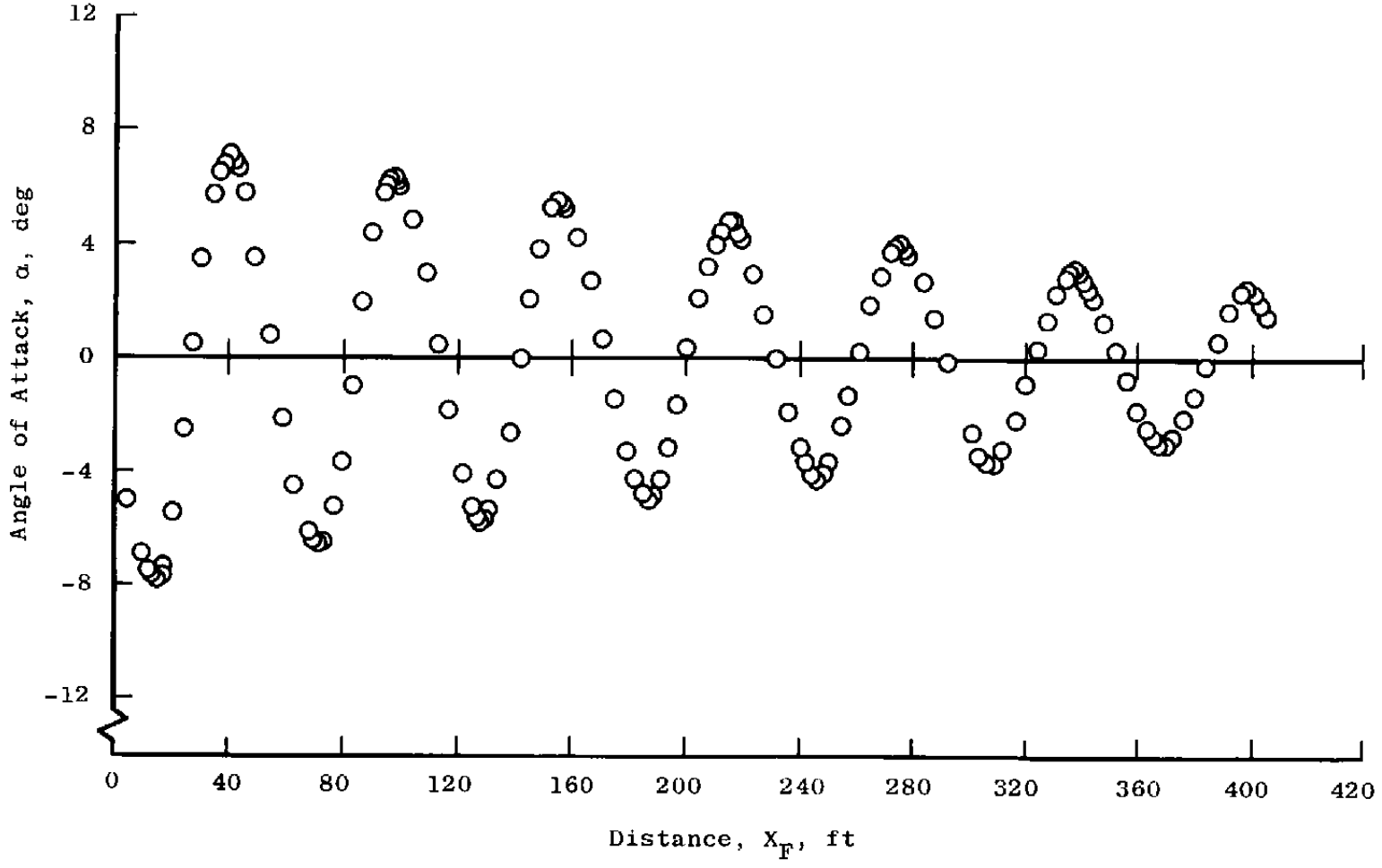

Fig. 26 Amplitude-Distance History

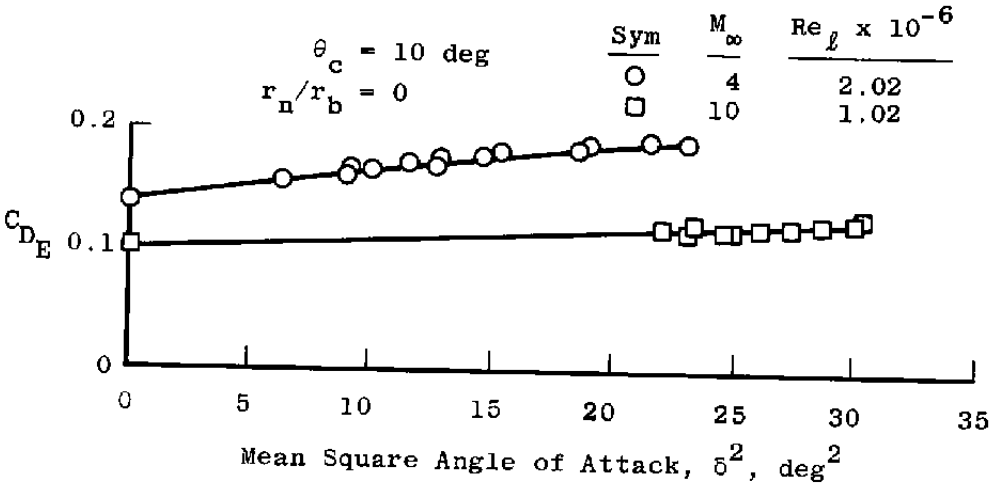

Fig. 27 Effective Total Drag Coefficient versus Mean Square Angle of Attack

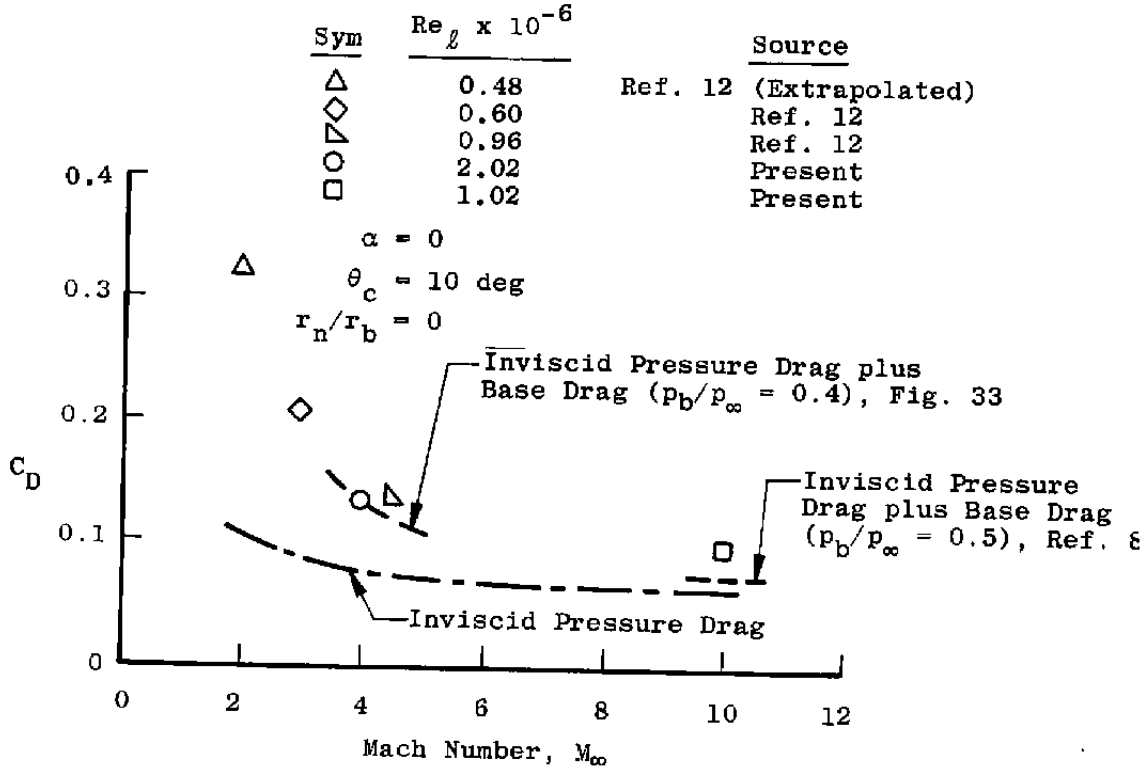

Fig. 28 Total Zero Angle-of-Attack Drag Coefficient versus Mach Number

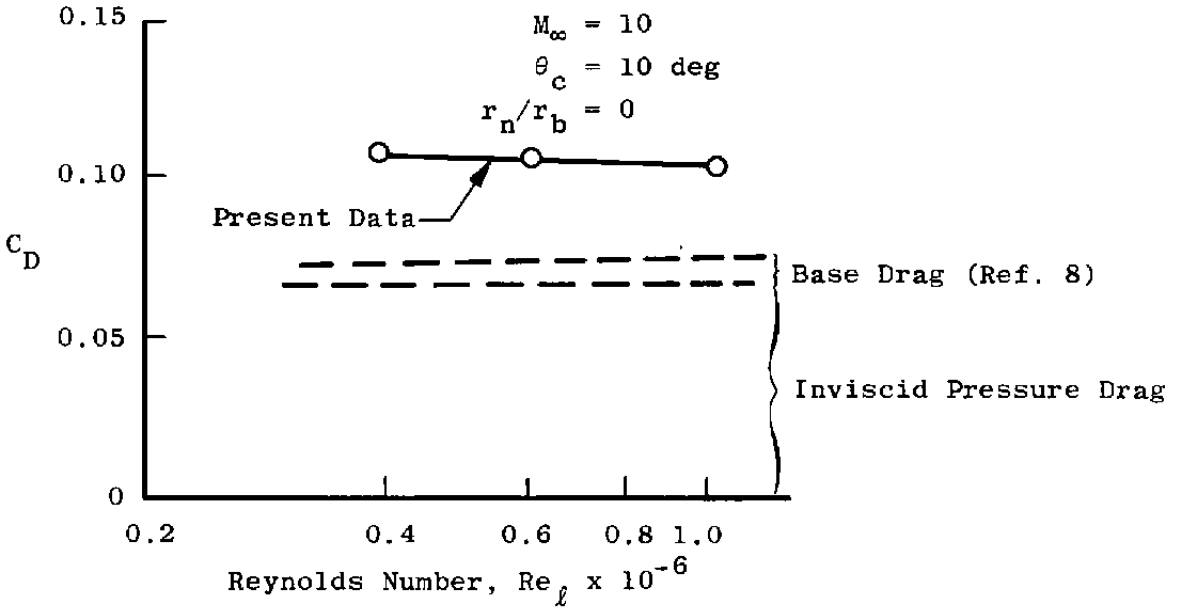

Fig. 29 Total Zero Angle-of-Attack Drag Coefficient versus Reynolds Number

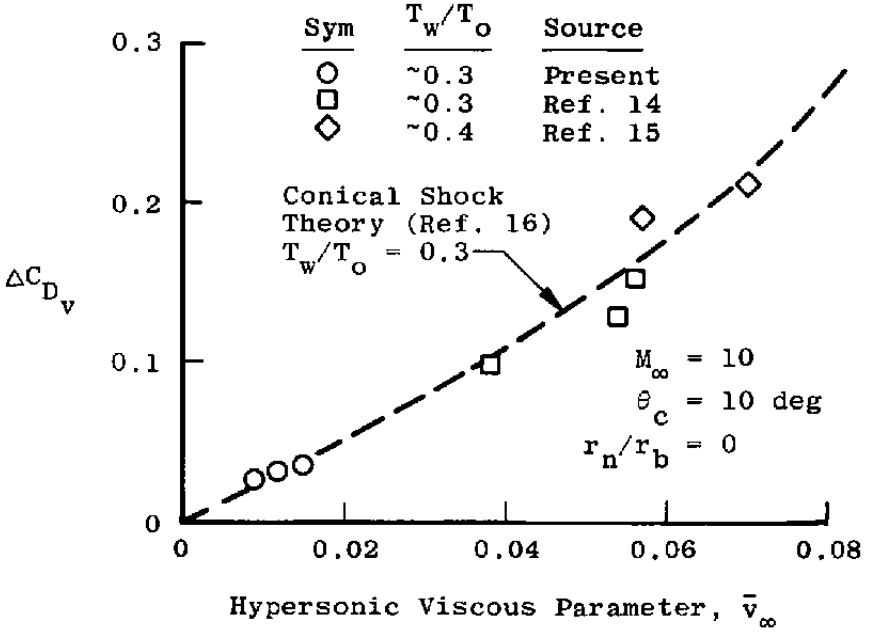

Fig. 30 Comparison of Theory and Free-Flight Drag Data, M_∞ = 10

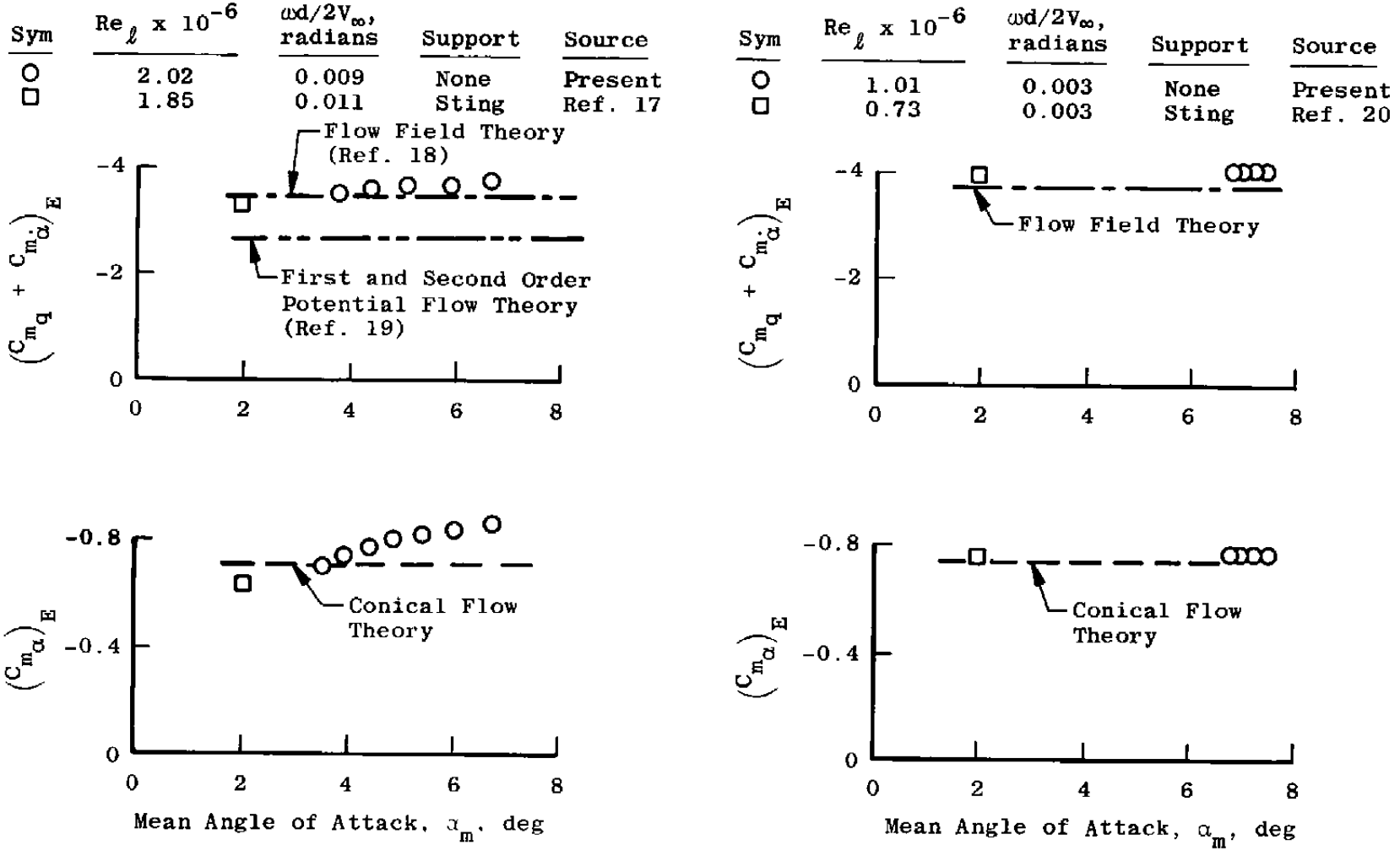

Fig. 31 Static and Dynamic Stability Derivatives versus Mean Angle of Attack at Mach 4 and 10

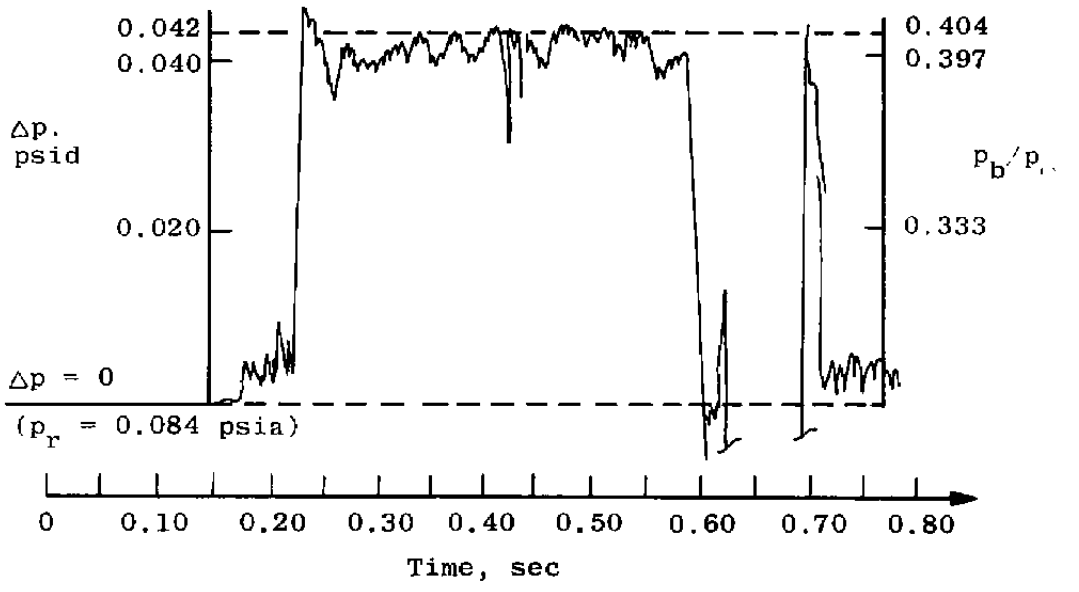

a. Nonoscillating Model

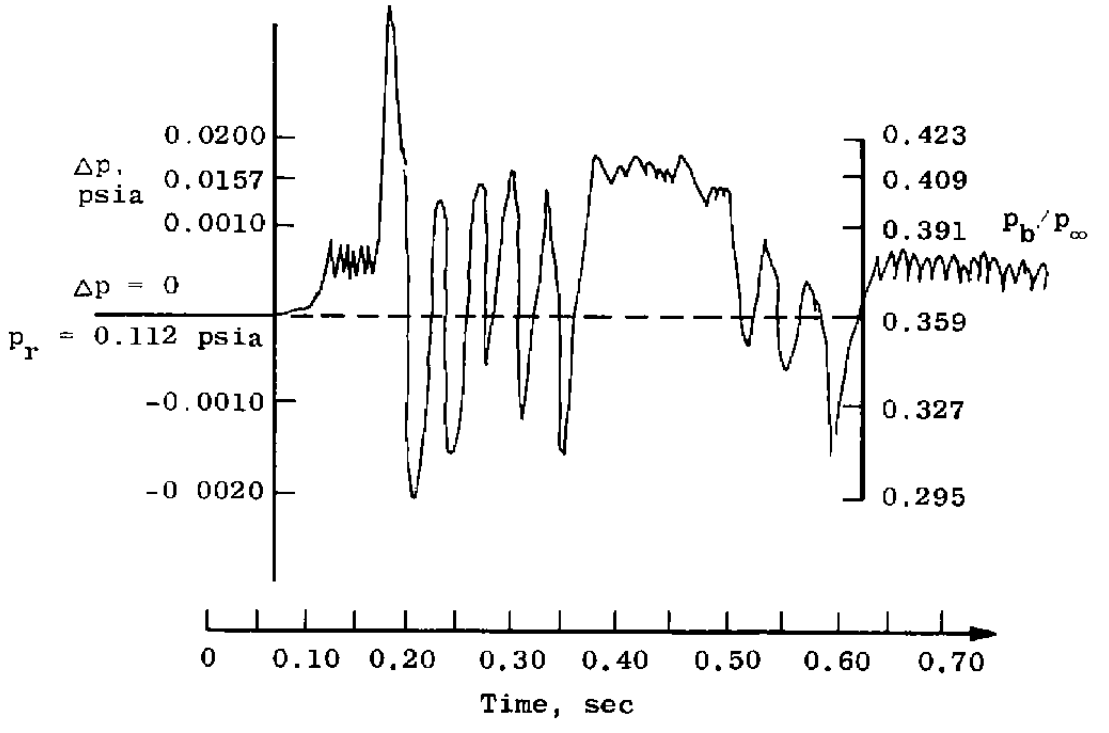

b. Oscillating Model

Fig. 32 Typical Oscillograph Traces of Model Base Pressure Variation (Δp), $M_\infty = 4$

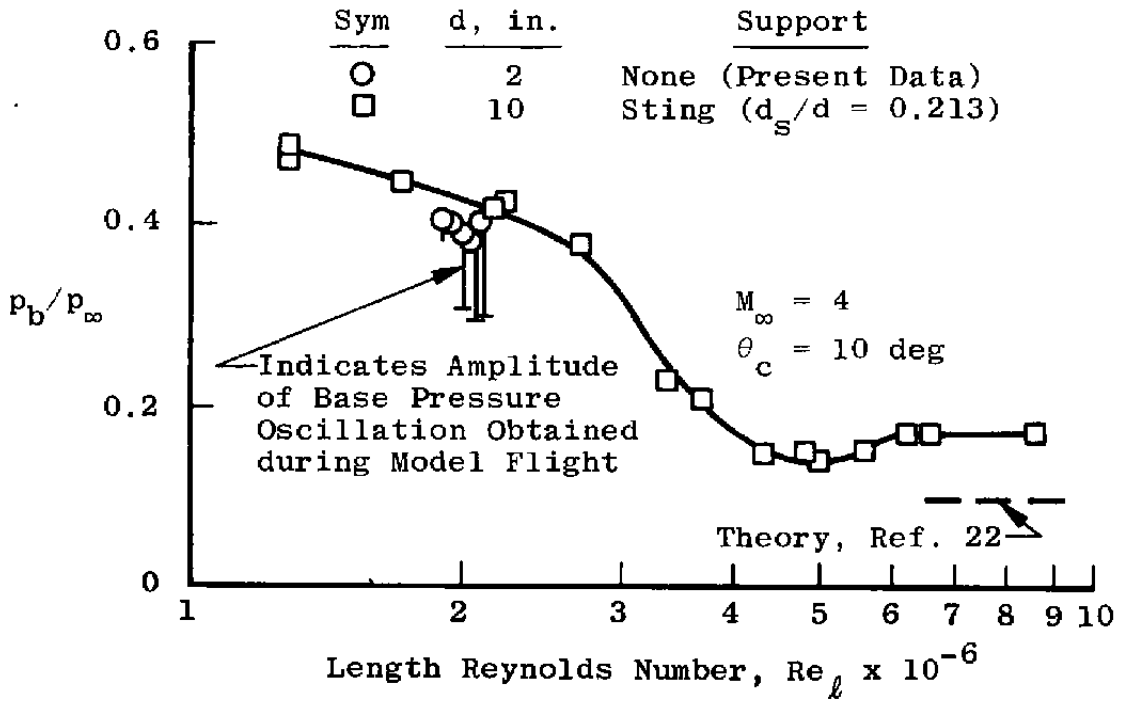

Fig. 33 Variation of Base Pressure Ratio with Reynolds Number

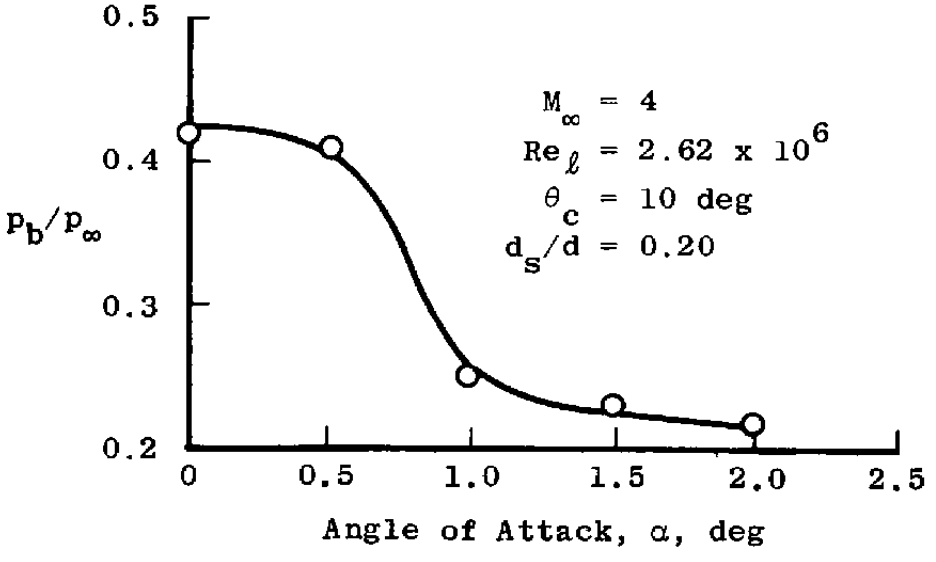

Fig. 34 Variation of Model Base Pressure with Angle of Attack, Sting-Supported Model

APPENDIX I
DERIVATIONS OF THE EQUATIONS OF MOTION

COORDINATE SYSTEMS

The equations of motion are developed using the axes systems shown in Fig. (I-1). Model position and orientation are determined relative to a media fixed coordinate system (X_F, Y_F, Z_F) in a manner analogous to that of a ballistic range. The X_T, Y_T, Z_T are the tunnel coordinates (inertial reference) and are fixed in space at $t = 0$. The X_m, Y_m, Z_m system has its origin fixed at the model center of mass and, like the media fixed system, remains parallel to the tunnel fixed system. The body axes (X, Y, Z) are fixed in the model with their origin at the center of mass. The angular orientation of this system relative to the X_m, Y_m, Z_m system and inertial space is given by the Euler angles ψ, θ, and ϕ. The origins of all four systems occupy the same point in space at $t = 0$.

Shown in Fig. (I-1) are the coordinate systems at $t > 0$. The horizontal distance X_F from the model center of gravity to the X_F, Y_F, Z_F system is defined as follows:

$$X_F = V_\infty t + X_T$$

Taking derivatives with respect to time yields expressions for velocity and acceleration referenced to the moving gas media

$$V_{X_F} = V_\infty + V_{X_T}$$

$$a_X = a_{X_T}$$

Note that the horizontal acceleration is equal in value for both the inertial and media fixed systems.

EQUATIONS OF MOTION

As is customary in the treatment of the motion of a rigid body, the equations of motion will be developed relative to the body fixed axes. The equations of motion derived from basic vector considerations are:

$$\frac{d\bar{M}}{dt} = \Sigma\bar{F}$$

$$\frac{d\bar{H}}{dt} = \Sigma\bar{M}$$

These equations are taken with respect to space fixed axes; therefore, it is necessary to transform them to account for the rotation of the body axes. This is done by using the well-known transformation for the rate of change of any vector from fixed to rotating axes as follows:

$$\frac{d\bar{M}}{dt} + \bar{\omega} \times \bar{M} = \Sigma\bar{F}$$

$$\frac{d\bar{H}}{dt} + \bar{\omega} \times \bar{\Pi} = \Sigma\bar{M}$$

The above equations may be written in the following scalar forms:

$$\begin{aligned}
&m(\dot{u} + qw - rv) = (\Sigma F)_X \\
&m(\dot{v} + ru - pw) = (\Sigma F)_Y \\
&m(\dot{w} + pv - uq) = (\Sigma F)_Z \\
&I_X\dot{p} + (I_Z - I_Y)rq - I_{XZ}(\dot{r} + qp) + I_{XY}(rp - \dot{q}) + I_{YZ}(r^2 - q^2) = (\Sigma M)_X \\
&I_Y\dot{q} + (I_X - I_Z)pr - I_{XY}(\dot{p} + rq) + I_{YZ}(pq - \dot{r}) + I_{XZ}(p^2 - r^2) = (\Sigma M)_Y \\
&I_Z\dot{r} + (I_Y - I_X)qp - I_{YZ}(\dot{q} + pr) + I_{XZ}(qr - \dot{p}) + I_{XY}(q^2 - p^2) = (\Sigma M)_Z
\end{aligned} \tag{I-1}$$

Roll, pitch, and yaw rates in the general case may be obtained from Fig. (I-1) as follows:

$$\begin{aligned}
p &= \dot{\phi} - \dot{\psi}\sin\theta \\
q &= \dot{\theta}\cos\phi + \dot{\psi}\cos\theta\sin\phi \\
r &= \dot{\psi}\cos\theta\cos\phi - \dot{\theta}\sin\phi
\end{aligned} \tag{I-2}$$

To begin the development of the equations of motion for a model oscillating in planar motion, it will be assumed that:

1. Model motion is confined to the X_TZ_T plane ($v = p = r = \psi = \phi = 0$),
2. Only first order linear aerodynamics exists,
3. The motion is described by α, q, and $\dot{\alpha}$, and
4. Model motion is limited to small angular excursions ($\alpha, \theta \ll 1$).

Assumption 1 reduces Eqs. (I-1) and (I-2) to

$$m(\dot{u} + qw) = (\Sigma F)_X \tag{I-3}$$

$$m(\dot{w} - uq) = (\Sigma F)_Z \tag{I-4}$$

$$I_Y \dot{q} = M_Y \tag{I-5}$$

$$q = \dot{\theta} \tag{I-6}$$

The aerodynamic forces and moments can be written using assumptions 2 and 3 as follows:

$$-F_X = F_A = \rho_\infty \frac{V^2 A}{2} C_A$$

$$-F_Z = F_N = \rho_\infty \frac{V^2 A}{2} \left\{ C_{N_o} + C_{N_\alpha} \alpha + C_{N_q} \left(\frac{qd}{2V}\right) + C_{N_{\dot{\alpha}}} \left(\frac{\dot{\alpha} d}{2V}\right) \right\}$$

$$M_Y = \rho_\infty \frac{V^2 A d}{2} \left\{ C_{m_o} + C_{m_\alpha} \alpha + C_{m_q} \left(\frac{qd}{2V}\right) + C_{m_{\dot{\alpha}}} \left(\frac{\dot{\alpha} d}{2V}\right) \right\}$$

Using Eqs. (I-3) through (I-6), assumption 4 (θ and $\alpha \ll 1$) and the above relations along with Fig. I-2, we can write

$$\dot{u} \simeq -\rho_\infty \frac{V^2 A}{2m} C_A \tag{I-7}$$

$$\dot{w} - uq \simeq -\rho_\infty \frac{V^2 A}{2m} \left\{ C_{N_o} + C_{N_\alpha} \alpha + C_{N_q} \left(\frac{\dot{\theta} d}{2V}\right) + C_{N_{\dot{\alpha}}} \left(\frac{\dot{\alpha} d}{2V}\right) \right\} + g \tag{I-8}$$

$$\ddot{\theta} = \rho_\infty \frac{V^2 A d}{2I} \left\{ C_{m_o} + C_{m_\alpha} \alpha + C_{m_q} \left(\frac{\dot{\theta} d}{2V}\right) + C_{m_{\dot{\alpha}}} \left(\frac{\dot{\alpha} d}{2V}\right) \right\} \tag{I-9}$$

In addition an equation involving drag may be written as:

$$\dot{V} \simeq -\rho_\infty \frac{V^2 A}{2m} C_D \tag{I-10}$$

The small angle assumption may be used to show the following:

$$u \simeq V \tag{I-11}$$

$$w \simeq \alpha V \tag{I-12}$$

and

$$\dot{u} \simeq \dot{V} \tag{I-13}$$

As shown by Eq. (I-13), Eqs. (I-7) and (I-10) are interchangeable For this development, it is preferred that Eq. (I-10) be used since drag is obtained directly from the free-flight tests. The equations of motion for a vehicle oscillating in free-flight planar motion are then Eqs. (I-8, -9, and -10).

Equation of Oscillatory Angular Motion

Differentiating Eq. (I-12) with respect to time yields

$$\dot{w} = \dot{\alpha}V + \alpha\dot{V}$$

Substituting this relation along with Eqs. (I-6, -10, and -11) into Eq. (I-8) we obtain

$$\left(1 - \rho_\infty \frac{Ad}{4m} C_{N_q}\right)\dot{\theta} = \left(1 + \rho_\infty \frac{Ad}{4m} C_{N_{\dot{\alpha}}}\right)\dot{\alpha} - \rho_\infty \frac{VA}{2m}\left(C_D - C_{N_\alpha}\right)\alpha + \rho_\infty \frac{VA}{2m} C_{N_0} - g/V$$

Since $\rho_\infty Ad/4m \simeq 10^{-3}$, we may reduce this expression to

$$\dot{\theta} = \dot{\alpha} - \rho_\infty \frac{AV}{2m}\left(C_D - C_{N_\alpha}\right)\alpha + \rho_\infty \frac{AV}{2m} C_{N_0} - g/V \qquad \text{(I-14)}$$

Taking a derivative with respect to time and substituting Eq. (I-10), we obtain

$$\ddot{\theta} = \ddot{\alpha} - \rho_\infty \frac{AV}{2m}\left(C_D - C_{N_\alpha}\right)\dot{\alpha} + \left(\rho_\infty \frac{AV}{2m}\right)^2\left(C_D - C_{N_\alpha}\right)C_D\alpha - \left(\rho_\infty \frac{AV}{2m}\right)^2 C_{N_0} C_D - \rho_\infty \frac{A}{2m} C_D g$$

Substituting the above equation and Eq. (I-14) into Eq. (I-9) gives the differential equation for planar oscillatory motion of a body in free flight

$$\ddot{\alpha} + C_1\dot{\alpha} + C_2\alpha = C_3 + C_4 \qquad \text{(I-15)}$$

where

$$C_1 = -\rho_\infty \frac{AV}{2m}\left[C_D - C_{N_\alpha} + \frac{I}{2}\left(\frac{d}{\sigma}\right)^2\left(C_{m_q} + C_{m_{\dot{\alpha}}}\right)\right]$$

$$C_2 = -\rho_\infty \frac{AV^2}{2md}\left[\left(\frac{d}{\sigma}\right)^2 C_{m_\alpha} - \rho_\infty \frac{Ad}{2m} C_D\left(C_D - C_{N_\alpha}\right) - \rho_\infty \frac{Ad}{4m}\left(\frac{d}{\sigma}\right)^2 C_{m_q}\left(C_D - C_{N_\alpha}\right)\right]$$

$$C_3 = \rho_\infty \frac{AV^2}{2md}\left[\left(\frac{d}{\sigma}\right)^2 C_{m_0} + \rho_\infty \frac{Ad}{2m} C_{N_0}\left\{\frac{1}{2}\left(\frac{d}{\sigma}\right)^2 C_{m_q} + C_D\right\}\right]$$

$$C_4 = -\rho_\infty \frac{Ag}{2m}\left[\frac{1}{2}\left(\frac{d}{\sigma}\right)^2 C_{m_q} - C_D\right]$$

$$\sigma = \sqrt{I/m}$$

Neglecting products of $\rho_\infty A/2m$, C_2 and C_3 reduce to

$$C_2 \simeq -\rho_\infty \frac{AV^2}{2md}\left(\frac{d}{\sigma}\right)^2 C_{m_\alpha}$$

$$C_3 \simeq \rho_\infty \frac{AV^2}{2md}\left(\frac{d}{\sigma}\right)^2 C_{m_0}$$

Equation (I-15) has variable coefficients attributable to the presence of V and cannot be solved easily. These variable coefficients are eliminated by changing the independent variable from time to distance according to the transformations

$$\dot{\alpha} = \frac{\partial \alpha}{\partial X_F}\frac{dX_F}{dt} = \alpha' V_{X_F} \simeq \alpha' V$$

$$\ddot{\alpha} = \frac{\partial^2 \alpha}{\partial X_F^2}\left(\frac{dX_F}{dt}\right)^2 + \frac{\partial \alpha}{\partial X_F}\frac{d^2X_F}{dt^2} \simeq \alpha'' V^2 - \rho_\infty \frac{V^2 A}{2m} C_D \alpha'$$

where it is assumed that $V_{X_F} \simeq V$.

Substituting these transformations into Eq. (I-15) we get

$$\alpha'' + D_1 \alpha' + D_2 \alpha = D_3 + D_4 \qquad \text{(I-16)}$$

where

$$D_1 = -\rho_\infty \frac{A}{2m}\left[2C_D - C_{N_\alpha} + \frac{1}{2}\left(\frac{d}{\sigma}\right)^2\left(C_{m_q} - C_{m_{\dot{\alpha}}}\right)\right]$$

$$D_2 \simeq -\rho_\infty \frac{A}{2m}\left(\frac{d}{\sigma}\right)^2 C_{m_\alpha}$$

$$D_3 \simeq \rho_\infty \frac{A}{2md}\left(\frac{d}{\sigma}\right)^2 C_{m_0}$$

$$D_4 = -\rho_\infty \frac{Ag}{2m}\left[\frac{1}{2}\left(\frac{d}{\sigma}\right)^2 C_{m_q} - C_D\right]\frac{1}{V^2}$$

Assuming that D_1 remains approximately constant, a solution to Eq. (I-16) for $C_{m_\alpha} < 0$ is given as

$$\alpha = -\frac{C_{m_o}}{C_{m_\alpha}} + \frac{\left[C_{m_q}/2 - \left(\frac{\sigma}{d}\right)^2 C_D\right]}{C_{m_\alpha}} \frac{g\ell}{V^2} - \alpha_o \, e^{-(D_1/2)X_F} \cos(\Omega X_F + \gamma) \qquad \text{(I-17)*}$$

where

$$\Omega = \sqrt{D_2}$$

is the angular distance frequency in radians/ft.

The first and second terms in Eq. (I-17) are the trim angle of attack and gravity induced angle of attack, respectively. In most cases of interest, the second term is negligible, and if we consider only models which have $C_{N_o} = C_{m_o} = 0$, then Eq. (I-16) reduces to

$$\alpha'' + D_1 \alpha' + D_2 \alpha = 0$$

and Eq. (I-17) becomes

$$\alpha = \alpha_o e^{-(D_1/2)X_F} \cos(\Omega X_F + \gamma) \qquad \text{(I-18)}$$

Using an exponentially damped oscillation (Fig. I-3) as predicted by the above equation, we can obtain expressions for the damping-in-pitch coefficients and the pitching-moment slope coefficient as follows:

$$D_1 = -2\Omega \ln R/2\pi \, C_{Y_R}$$

where

$$R = \alpha_n/\alpha_o \text{ and } C_{Y_R} = \Omega \Delta X_F/2\pi$$

$$C_{m_q} + C_{m_{\dot\alpha}} = 2\left(\frac{\sigma}{d}\right)^2 \left[\frac{-2mD_1}{\rho_\infty A} - 2C_D + C_{N_\alpha}\right]$$

$$C_{m_\alpha} = -\frac{2md}{\rho_\infty A}\left(\frac{\sigma}{d}\right)^2 \Omega^2$$

EQUATIONS OF TRANSLATIONAL MOTION

Drag Deceleration

The differential equation defining the deceleration of a model in free flight was given previously as Eq. (I-10). Using the small angle

*A similar result is obtained in Ref. 21.

assumption and acceleration relative to the tunnel fixed coordinate system, we obtain the drag coefficient from this equation as follows:

$$C_D = \frac{2m}{\rho_\infty V_{X_F}^2 A} a_{X_T}$$

An alternate form of Eq. (I-10) referenced to the media fixed coordinate system is obtained by transforming the independent variable from time to distance according to the transformation

$$\dot{V} = \frac{\partial V}{\partial X_F}\left(\frac{dX_F}{dt}\right) = -\rho_\infty \frac{V^2 A}{2m} C_D$$

By assuming that $V \simeq V_{X_F}$ the drag coefficient is given as

$$C_D = \frac{-2m}{\rho_\infty A} \frac{\partial}{\partial X_F}\left(ln \frac{V_{X_F}}{C}\right)$$

where C is an arbitrary constant velocity. Let $C = V_\infty$ and recalling that $V_{X_F} = V_\infty + V_{X_T}$ then

$$C_D = \frac{-2m}{\rho_\infty A} \frac{\partial}{\partial X_F}\left[ln\left(1 + \frac{V_{X_T}}{V_\infty}\right)\right]$$

EFFECTIVE AND MEAN OSCILLATION AMPLITUDE

Free-flight data are extracted from the damped oscillatory amplitude-distance history over certain distance intervals (ΔX_F) as shown in Fig. (I-3). These data, therefore, represent effective values for the range of angle of attack encountered in this interval. For purposes of data correlation and presentation it is desirable to define both the effective angle of attack and the mean envelope amplitude for the data interval.

The effective angle of attack is defined to be the root-mean-square angle for the oscillation as follows:

$$\delta = \left\{\frac{1}{X_F}\int_0^{X_F} \alpha^2 dX_F\right\}^{1/2}$$

The limits 0 to X_F were chosen to represent the data interval in order to simplify the final form of δ (see Ref. 12). These limits do not restrict the use of this relation since distance is relative.

A general form of the effective angle of attack (δ) for an exponentially damped planar oscillation is obtained by substituting Eq. (I-18) into the above relation and integrating as follows:

$$\delta = \left\{ \frac{a_o^2}{X_F} \int_0^{X_F} e^{-D_1 X_F} \cos^2 (\Omega X_F + \gamma)\, dX_F \right\}^{1/2}$$

$$\delta = \left\{ \frac{a_o^2\, e^{-D_1 X_F}}{4[(D_1/2)^2 + \Omega^2] X_F} \frac{\Omega^2}{} \left[\frac{D_1}{\Omega^2} \cos^2 (\Omega X_F + \gamma) - \frac{2}{\Omega} \sin 2(\Omega X_F + \gamma) - \frac{2}{D_1} \right] \Bigg|_0^{X_F} \right\}^{1/2}$$

This result is greatly simplified by assuming that $|\Omega| >> |D_1|$, which is an accurate assumption for the cases of interest. The above result, therefore, becomes

$$\delta = \left\{ \frac{-a_o^2\, e^{-D_1 X_F}}{2 D_1 X_F} \right\}^{1/2}$$

From Fig. (I-3), we can see that for the interval X_{F_o} to X_{F_n} (0 to X_F) the damping factor is given as

$$D_1 = -2 \ln |a_n/a_o| / X_F$$

Substituting this relation into the previous one yields the desired general form for δ over a given distance interval ΔX_F

$$\delta = \left\{ \frac{a_n^2 - a_o^2}{4 \ln |a_n/a_o|} \right\}^{1/2} \qquad \text{(I-19)}$$

The mean amplitude of the same distance interval is given as

$$a_m = \sqrt{2\delta^2} = \left\{ \frac{a_n^2 - a_o^2}{2 \ln |a_n/a_o|} \right\}^{1/2}$$

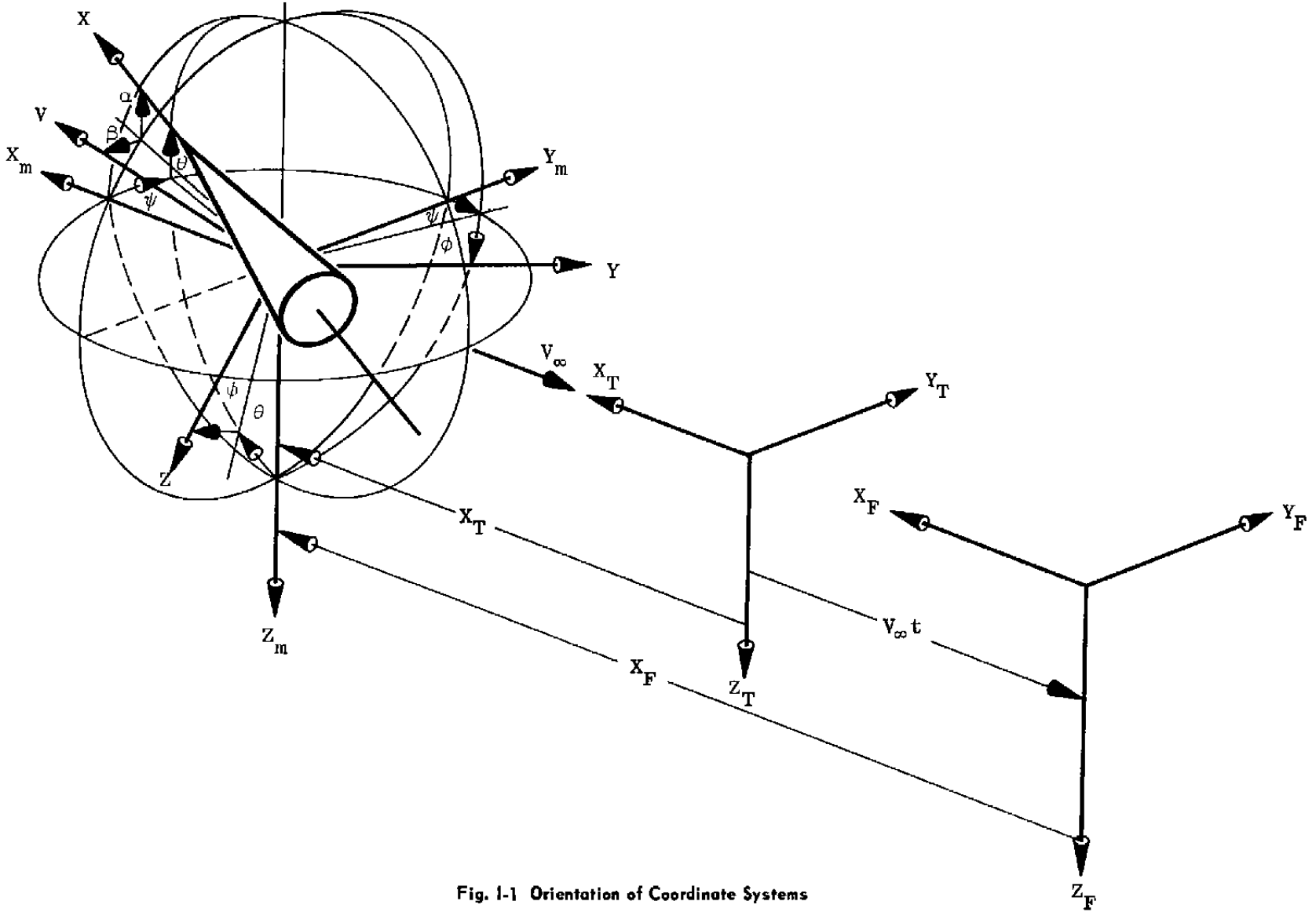

Fig. 1-1 Orientation of Coordinate Systems

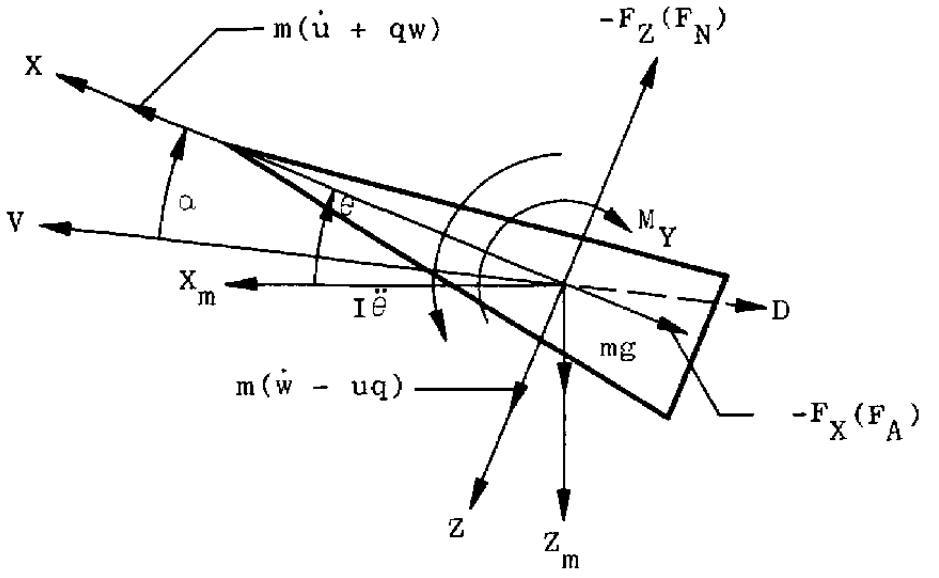

Fig. I-2 Forces and Moments in the $X_T Z_T$ Plane

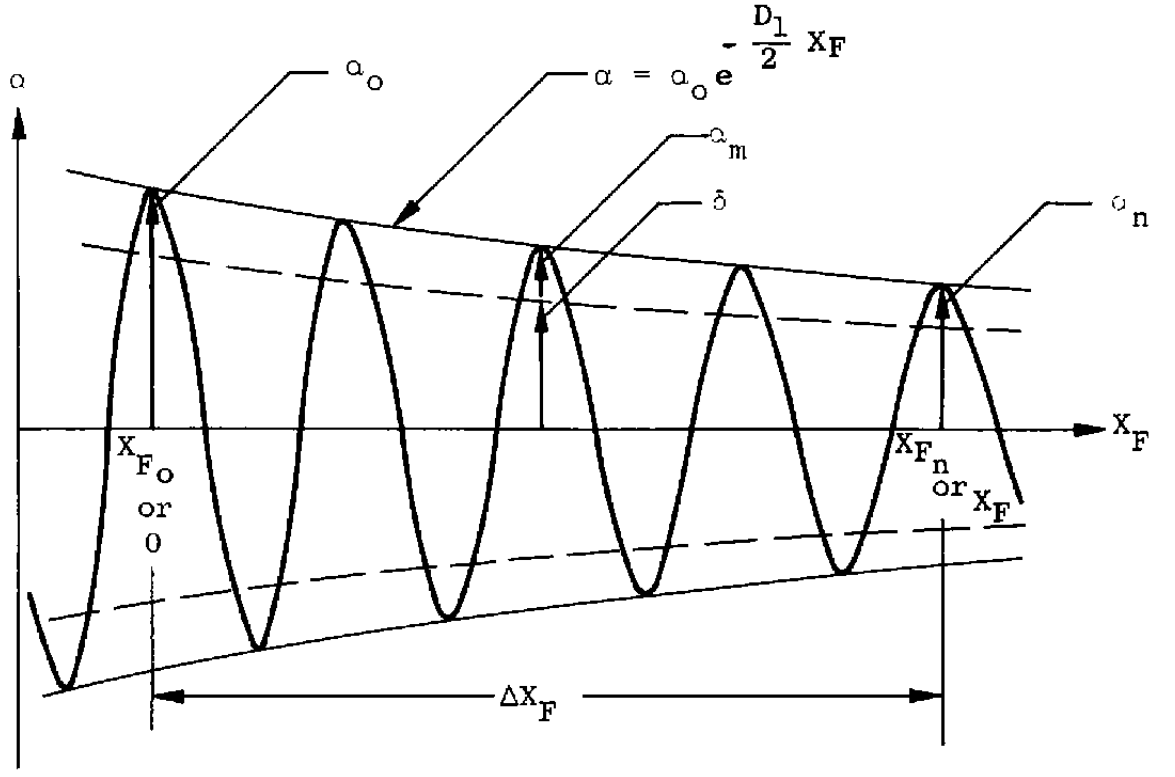

Fig. I-3 Data Interval

UNCLASSIFIED
Security Classification

DOCUMENT CONTROL DATA - R&D
(Security classification of title, body of abstract and indexing annotation must be entered when the overall report is classified)

1 ORIGINATING ACTIVITY (Corporate author)
Arnold Engineering Development Center,
ARO, Inc., Operating Contractor,
Arnold Air Force Station, Tennessee

2a REPORT SECURITY CLASSIFICATION
UNCLASSIFIED

2b GROUP
N/A

3 REPORT TITLE
DESCRIPTION OF A MODEL LAUNCHER AND TECHNIQUES USED FOR OBTAINING MODEL FREE-FLIGHT MEASUREMENTS IN THE VKF CONTINUOUS FLOW WIND TUNNELS AT MACH NUMBERS FROM 1.5 THROUGH 10

4 DESCRIPTIVE NOTES (Type of report and inclusive dates)
N/A

5 AUTHOR(S) (Last name, first name, initial)
Ward, L. K., Hodapp, A. E., Jr., and Choate, R. H., ARO, Inc.

6 REPORT DATE	7a TOTAL NO. OF PAGES	7b NO OF REFS
August 1966	71	22

8a CONTRACT OR GRANT NO.	9a ORIGINATOR'S REPORT NUMBER(S)
AF40(600)-1200	
b. Program Element 65402234	AEDC-TR-66-112
c.	9b OTHER REPORT NO(S) (Any other numbers that may be assigned this report)
d	N/A

10. AVAILABILITY/LIMITATION NOTICES
Qualified users may obtain copies of this report from DDC, and release to foreign governments or foreign nationals must have prior approval of AEDC.

11 SUPPLEMENTARY NOTES	12. SPONSORING MILITARY ACTIVITY
N/A	Arnold Engineering Development Center, Air Force Systems Command, Arnold Air Force Station, Tennessee

13 ABSTRACT

A model launcher has been developed for use in the continuous flow wind tunnels, Tunnels A, B, and C (Mach numbers from 1.5 through 10) of VKF. Support-free model drag, damping, and pitching-moment rate data may be obtained throughout the Mach number range. Model base pressure data, using onboard telemetry, may be obtained at Mach numbers up through 6. Repeated model launchings may be made without interrupting the tunnel flow. A description of the model launcher and testing procedures are presented with representative drag, damping, pitching-moment rate, and base pressure data obtained on 10-deg, half-angle cone models in free flight.

DD FORM 1 JAN 64 1473

UNCLASSIFIED
Security Classification

14 KEY WORDS	LINK A		LINK B		LINK C	
	ROLE	WT	ROLE	WT	ROLE	WT
model launchers						
conical models						
free-flight measurements						
drag						
damping						
pitching moment						
base pressure						
supersonic flow						
hypersonic flow						

INSTRUCTIONS

1. ORIGINATING ACTIVITY: Enter the name and address of the contractor, subcontractor, grantee, Department of Defense activity or other organization *(corporate author)* issuing the report.

2*a*. REPORT SECURITY CLASSIFICATION: Enter the overall security classification of the report. Indicate whether "Restricted Data" is included. Marking is to be in accordance with appropriate security regulations.

2*b*. GROUP: Automatic downgrading is specified in DoD Directive 5200.10 and Armed Forces Industrial Manual. Enter the group number. Also, when applicable, show that optional markings have been used for Group 3 and Group 4 as authorized

3. REPORT TITLE: Enter the complete report title in all capital letters. Titles in all cases should be unclassified. If a meaningful title cannot be selected without classification, show title classification in all capitals in parenthesis immediately following the title.

4. DESCRIPTIVE NOTES: If appropriate, enter the type of report, e.g., interim, progress, summary, annual, or final. Give the inclusive dates when a specific reporting period is covered.

5. AUTHOR(S): Enter the name(s) of author(s) as shown on or in the report. Enter last name, first name, middle initial. If military, show rank and branch of service. The name of the principal author is an absolute minimum requirement.

6. REPORT DATE: Enter the date of the report as day, month, year; or month, year. If more than one date appears on the report, use date of publication.

7*a*. TOTAL NUMBER OF PAGES: The total page count should follow normal pagination procedures, i.e., enter the number of pages containing information.

7*b*. NUMBER OF REFERENCES: Enter the total number of references cited in the report.

8*a*. CONTRACT OR GRANT NUMBER: If appropriate, enter the applicable number of the contract or grant under which the report was written.

8*b*, 8*c*, & 8*d*. PROJECT NUMBER: Enter the appropriate military department identification, such as project number, subproject number, system numbers, task number, etc.

9*a*. ORIGINATOR'S REPORT NUMBER(S): Enter the official report number by which the document will be identified and controlled by the originating activity. This number must be unique to this report.

9*b*. OTHER REPORT NUMBER(S): If the report has been assigned any other report numbers *(either by the originator or by the sponsor)*, also enter this number(s).

10. AVAILABILITY/LIMITATION NOTICES: Enter any limitations on further dissemination of the report, other than those imposed by security classification, using standard statements such as:

(1) "Qualified requesters may obtain copies of this report from DDC."

(2) "Foreign announcement and dissemination of this report by DDC is not authorized."

(3) "U. S. Government agencies may obtain copies of this report directly from DDC. Other qualified DDC users shall request through

_____."

(4) "U. S. military agencies may obtain copies of this report directly from DDC. Other qualified users shall request through

_____."

(5) "All distribution of this report is controlled. Qualified DDC users shall request through

_____."

If the report has been furnished to the Office of Technical Services, Department of Commerce, for sale to the public, indicate this fact and enter the price, if known.

11. SUPPLEMENTARY NOTES: Use for additional explanatory notes.

12. SPONSORING MILITARY ACTIVITY: Enter the name of the departmental project office or laboratory sponsoring *(paying for)* the research and development. Include address.

13. ABSTRACT: Enter an abstract giving a brief and factual summary of the document indicative of the report, even though it may also appear elsewhere in the body of the technical report. If additional space is required, a continuation sheet shall be attached.

It is highly desirable that the abstract of classified reports be unclassified. Each paragraph of the abstract shall end with an indication of the military security classification of the information in the paragraph, represented as *(TS), (S), (C), or (U)*

There is no limitation on the length of the abstract. However, the suggested length is from 150 to 225 words.

14. KEY WORDS: Key words are technically meaningful terms or short phrases that characterize a report and may be used as index entries for cataloging the report. Key words must be selected so that no security classification is required. Identifiers, such as equipment model designation, trade name, military project code name, geographic location, may be used as key words but will be followed by an indication of technical context. The assignment of links, rules, and weights is optional.